Probing the conformational dynamics of an OTU deubiquitinase enzyme active site

by

Roy Hutchings

A Thesis submitted to the Faculty of Graduate Studies of
University of Manitoba
in partial fulfilment of the requirements for the degree of

Master of Science

Department of Chemistry
University of Manitoba
Winnipeg, Manitoba

Abstract

Enzymes are fundamental to cell function. Despite this, exactly how they work remains unclear. Enzymes exist as 3D folded structures determined by their amino acid sequence, and these structures are necessary for function. However, enzymes change their 3D conformation frequently during the course of a reaction, and an understanding of these dynamic motions is necessary for a complete understanding of enzyme function. As a model for enzyme dynamics, we have studied the catalytic domain of Otu1, an ovarian tumour domain-containing deubiquitinase from yeast *Saccharomyces cerevisiae*. Deubiquitinases catalyze the breakdown of ubiquitin, and play an important role in regulating cell functions including immune response and signal transduction. We have probed the structural dynamics of the catalytic domain of Otu1 using the cysteine-labelling molecule 4,4'-dithiodipyridine (DTDP). The labelling reaction kinetics have been followed using stopped-flow fluorescence spectroscopy methods and have revealed the presence of a conformational change with a frequency of $127 \pm 7\ s^{-1}$. This conformational change may potentially play a role in the enzyme's catalytic mechanism.

Acknowledgements

My advisor, Dr. Mazdak Khajehpour;

The members of my advisory committee, Dr. Brian Mark and Dr. Hélène Perreault;

All members of the Mark lab, especially Ben Bailey-Elkin and Veronica Larmour for their help with cloning;

All members of the Khajehpour lab: Ian Reinhorn, Shin Young Park, Tania Ghuman, Jaryd Sullivan, Olga Francisco, Courtney Clark, Hayden Glor, and Ryan Macdonald for their help, support, and entertainment;

Especially Ian Reinhorn, for acquiring helpful absorbance spectra; Shin Young Park, for running the DSC traces and SDS-PAGE gel shown in this thesis; and Tania Ghuman, for measuring one of the enzyme activity trials in this thesis;

Dr. Stephanie Portet, for her help with mathematical analysis;

Dr. Joe O'Neil and Vu To, for training with and use of their CD spectropolarimeter;

And the Oresnik lab, for use of their centrifuge.

Dedication

This thesis is dedicated to all my teachers, past and present, and especially to my parents.

Table of Contents

List of Tables

List of Figures

List of Abbreviations

4-TP	4-Thiopyridone
AMC	7-amino-4-methylcoumarin
C_2H_2	Cys_2His_2
CD	Circular dichroism
CPMG	Carr-Purcell-Meiboom-Gill
DSC	Differential scanning calorimetry
DTDP	4,4'-Dithiodipyridine
DTNB	5,5'dithio-bis(2-nitrobenzoic acid)
DTT	Dithiothreitol
DUB	Deubiquitinase
EDTA	Ethylenediaminetetraacetic acid
IPTG	Isopropyl β-D-1-thiogalactopyranoside
NACA	N-acetylcysteine amide
NMR	Nuclear magnetic resonance
OTU	Ovarian tumour
RET	Resonance energy transfer
SDS	Sodium dodecyl sulfate
T.S.	Transition state
TRIS	Tris(hydroxymethyl)aminomethane
Ub	Ubiquitin
UBX	Ubiquitin-like fold
ZN	Putative zinc-binding or C_2H_2 domain

1. Introduction

1.1. ENZYMES AND ENZYME DYNAMICS

Proteins are polymers of amino acids synthesized by cells to carry out a variety of functions. Enzymes are a subset of proteins that catalyze biochemical reactions. As catalysts, they function to increase the rate of a reaction – simple biochemical reactions that could take years to complete can be reduced to a matter of seconds in the presence of enzymes[1,2]. Typically, an enzyme carries out its reaction on a specific substrate. Multiple enzymes often work sequentially in a series of reactions to carry out complex biochemical processes such as degradation of nutrients or construction of cellular structures[3,4]. The enzymes allow the process to both occur at a useful timescale, as well as be organized and finely controlled[3]. Enzymes play significant and fundamental roles in virtually every aspect of cell function, including metabolism, motility, homeostasis, and replication[3]. As a result, they are often the targets of drug design methodologies[5]. Deficiency, absence, or excess of a single enzyme can sometimes lead to disease or death of the entire organism[6]. We simply cannot live without them.

However, despite their fundamental importance to virtually every aspect of life, exactly how enzymes work still remains unclear. Under physiological conditions, proteins exist as 3D folded structures determined by their amino acid sequence[3,7]. These structures are necessary for their function[8,9]. Solving these structures using methods such as X-ray crystallography or nuclear magnetic resonance spectroscopy has become ubiquitous in characterizing enzymes. Typically, these methods provide structural information about the single most stable enzyme conformation under experimental conditions[10,11]. They have provided great insight into protein function at the molecular level. For example, it has been shown that most enzyme structures contain a pocket

called the “active site” within which the chemical reaction takes place[12,13]. The surface of the active site is lined with amino acid residues organized to both promote binding of the substrate(s) to the pocket and participate in the catalytic chemistry of the reaction[12].

An idea proposed by Haldane[14], and elaborated upon by Pauling[15], applies transition state theory to explain enzyme catalysis. The transition state (T.S.) is the highest energy point of a chemical reaction, from where collapse to products or reactants is equally likely[16]. The activation energy is the difference in energy between the T.S. and the reactants in the ground state, and is directly related to the rate of the reaction (a smaller activation energy means a faster reaction)[16]. In this model, the structure of the enzyme active site is organized such that favourable weak interactions stabilize the T.S. relative to the substrates, resulting in a lowered activation energy and faster reaction[17]. This explanation has historically been popular, is taught in many textbooks[17], and explains the remarkably tight binding of unreactive analogs of T.S. structures to their respective enzymes[18-20] (with dissociation constants down to the femtomolar range![21]). Unfortunately, it fails to fully describe enzyme function, as artificial enzymes designed to bind favourably to transition state mimics (and therefore the transition state of the reaction) do not achieve anywhere close to the same level of rate enhancement as natural enzymes[22,23]. By focusing on a static active site structure, this theory ignores the contributions of dynamic changes in the proteins structure. In fact, it is now well known that enzymes do not exist as a single structure, but instead change their 3D conformation constantly during the course of a reaction[1,10].

A large body of theoretical and experimental studies show that enzyme structural fluctuations occur over a range of time scales, from femtoseconds to minutes, and involve the vibrations of individual bonds up to the motions of large domains[10,24]. Bond vibrations and the T.S. lifetime

both occur on the femtosecond to picosecond timescale[23,25]. Computational simulations have suggested that rather than statically stabilizing a T.S. structure, enzymes may utilize specific bond vibrations on this timescale to promote reactants to cross the activation energy barrier[23,25]. This idea has been supported by the study of "heavy enzymes", in which an enzyme's amino acids are uniformly labelled with heavier isotopes of the same atoms, resulting in an enzyme which retains the same electrostatics yet has altered bond vibrations on the femtosecond to picosecond timescale[26,27]. In such heavy enzymes, the chemical step of catalysis is slower than in the corresponding light enzymes[26,27]. Larger fluctuations such as loop motions and side chain rotations usually occur on the picosecond to nanosecond timescale[10]. They can be involved in regulating catalytic activity[28]. Evidence suggests that these frequent thermal fluctuations collectively facilitate comparatively rarer and larger-scale conformational changes[29,30]. Significant conformational changes and domain motions usually occur on the timescale of microseconds to milliseconds[24], which is the typical rate of catalytic turnover[10]. This is not a coincidence. For example, during a reaction, enzymes must change conformation from a binding incompetent form to a form allowing substrate binding[31-34]; once substrate is bound they may relax into a catalytic form[28,32,35,36]; and finally, once the product is made, they must adopt a form allowing separation of the product[32,33,37]. Depending on the enzyme, more or fewer steps may be involved[38].

The connection between catalytic turnover and structural dynamics has been experimentally demonstrated[1,29,39]. For example, in the catalytic cycle of human cyclophilin A, substrate binding, catalysis, and product release are each accompanied by a distinct conformational change on the high-microsecond timescale[39]. Interestingly, these conformational changes involve

"networks" of concerted motions across the global protein structure[40], and are sampled by the free enzyme before catalysis[33,40]. As another example, the structure of *Escherichia coli* adenylate kinase contains two "lids" that close upon binding of substrate, and opening of these lids on the millisecond timescale appears to be the rate-limiting step for catalysis by this enzyme[32].

The structure of an enzyme may be best described as a "hierarchy or ensemble of interconverting conformations"[1]. It is clear that the structure of a single conformation will provide incomplete information about the process of enzyme catalysis. Therefore, in order to completely understand how enzymes function, we must also understand their dynamics – their changes in conformation over time.

1.2. HOW ENZYME DYNAMICS ARE STUDIED

There is a myriad of methods used to study the dynamic properties of biological molecules. Two of the most successful tools are nuclear magnetic resonance (NMR) spectroscopy and time-resolved kinetic methods. NMR spectroscopy utilizes the magnetic properties of some atoms to elucidate information about molecular structure and dynamics. NMR-active nuclei act as reporters of their unique local chemical environment, and signals from multiple nuclei in the molecule are simultaneously recorded in an NMR experiment[41]. This allows detailed structural information to be acquired at atomic resolution[41,42]. Changes in enzyme conformation and dynamic motions usually alter the chemical environment of nuclei, and this is reflected by changes in chemical shift, intensity, and linewidth (or transverse relaxation rate) of signals from the affected nuclei[42]. How this manifests on an NMR spectrum depends on the relative rates of conformational exchange and chemical shift. If interconversion is slow, then distinct signals are observed for each conformational state[42]. In this case, the structure of each species can be

characterized, and the relative populations can be determined from comparison of the peak intensities[29]. As well, magnetization exchange spectroscopy can be performed to measure the forward and reverse rate constants of interconversion if they are on the millisecond to second timescale [41,43,44]. As the rates of exchange between the interconverting species approaches or exceeds the difference in their chemical shift (expressed in frequency units), the signals broaden or converge to one population-averaged signal[42]. Microsecond to millisecond dynamics can cause fluctuations in the chemical shift of the converged signal and can be characterized by Carr-Purcell-Meiboom-Gill (CPMG) relaxation dispersion experiments[41,45]. CPMG can also be a powerful tool for determining enzyme structures, including those of low-population conformers[46]. Dynamics on the picosecond to nanosecond timescales can be characterized using residual dipolar couplings and spin relaxation measurements[38,41,47,48].

While NMR usually observes conformational dynamics at equilibrium, time-resolved kinetic methods initiate a fast perturbation of an enzyme system and follow its relaxation to a new equilibrium over time using a structural probe, usually optical spectroscopy[24]. Once measured, relaxation times are fit to a kinetic model and rate constants for the transition are obtained. Typically, kinetic methods are able to either provide support for or rule out different dynamic models for the structural or chemical transition being studied and allow the timescales of enzyme conformational interconversion to be determined[24].

For example, temperature-jump (T-jump) methods induce a fast increase in temperature within nanoseconds or microseconds (usually a change of around 10 ºC), and relaxation of the system to the new equilibrium can be followed throughout a large range of timescales (nanoseconds to seconds or longer)[24,49-52]. T-jump is simple and applicable to a wide variety of systems, as long

as there is at least a small difference in enthalpy between the conformations of interest[24]. A variety of laser-induced pH-jump reagents (such as o-nitrobenzaldehyde) can be used to perturb pH-sensitive reactions by altering the pH by up to 1-5 units within nanoseconds[53] and lasting for a microsecond or longer[53-55]. In these reagents, the acid dissociation constant of the electronically excited-state is significantly higher or lower than that of the ground state, such that protons are effectively emitted or taken up upon excitation by a photon[24]. In a similar way, rapid-mixing techniques permit the study of enzyme structural changes that occur upon reaction with substrate. Stopped flow methods are capable of mixing enzyme and substrate solutions within a millisecond and so are ideally suited for dynamics on this timescale or longer[56]. Continuous flow is another rapid-mixing technique with microsecond time resolution[57], and although traditionally large sample volumes are required[58], modern continuous flow setups using microfluidic cells need less sample[59,60].

Perturbation methods must be combined with a probing technique to monitor the resulting structural changes. Spectroscopic techniques including fluorescence, infra-red (IR), and UV-vis absorbance are the structural probes most commonly used for this purpose. Many proteins contain one or more tryptophan residues, and fluorescence of the indole ring is quite sensitive to changes in its local environment[61-63]. In the absence of tryptophan, tyrosine may also be used as an intrinsic fluorescent probe[64]. Alternatively, enzymes can be labelled with a variety of extrinsic probes sensitive to changes in different properties[61,65]. Importantly, the change in distance between two points on a protein over time can be measured using resonance energy transfer (RET), including at the single molecule level[66,67]. IR spectroscopy can detect changes in protein secondary structure, H-bonding, and side-chain orientation, solvation, and packing[24]. As well,

many proteins contain cofactors or functional groups such as hemes or NAD(P)H that exhibit absorbance in the UV-Vis region and that are sensitive to chemical or structural changes[24]. Regardless of the perturbation method used, UV-Vis absorbance and IR spectroscopy are both inherently capable of time resolution down to picoseconds, while the limit of fluorescence is usually nanoseconds[24]. As an alternative to optical methods, detection by on-line mass-spectrometry offers the potential to distinguish between all species in solution simultaneously, but is limited by time resolution down to milliseconds[68].

Optical time-resolved kinetic methods have poor structural resolution, but are very sensitive, usually require small amounts of sample, and provide excellent time resolution. A single experiment is capable of following the dynamics of a process over a wide range of timescales, for example from nanoseconds to seconds or longer. In contrast, NMR spectroscopy grants atomic-scale structural resolution, but each experiment provides a narrow dynamic timescale range. Both techniques allow data acquisition in solution. NMR spectroscopy collects data without significant perturbation of the enzyme system[41,69], although is limited to smaller proteins[69], requires larger amounts of sample[42], and the proteins must usually be substituted with NMR-active nuclei[70]. Finally, despite the strength and abundance of techniques available for studying the dynamics of biomolecules, interpreting these data is helped immensely when snapshots of enzyme structure are available through methods such as X-ray crystallography, small-angle x-ray scattering, or NMR spectroscopy.

1.3. DEUBIQUITINASES AND THE UBIQUITIN SYSTEM

We have studied the dynamics of Otu1, a deubiquitinase enzyme active in the ubiquitin system. Ubiquitin is a small (76 amino acid) protein covalently attached to other proteins as a reversible post-translational modification for signalling purposes. Ubiquitin can be attached as a monomer

or as a chain. In ubiquitin chains, an isopeptide bond is formed between the C-terminal carboxyl group of the distal ubiquitin and one of seven lysine ε-amino groups of the preceding ubiquitin (Lys6, Lys 11, Lys 27, Lys29, Lys33, Lys48, or Lys63)[71,72]. In such chains, the type of linkage between the ubiquitin molecules specifies the signal conveyed. For example, chains in which each ubiquitin is attached to Lys48 of the preceding ubiquitin usually flag their substrate to be degraded by the proteasome[73], while Lys63-linked chains are involved in other signalling functions such as DNA repair[74] and endocytosis[75]. Ubiquitinases (or E3-ligases) are responsible for extending or adding ubiquitin chains to target molecules, while deubiquitinases (DUBs) remove or shorten them. DUBs therefore play a crucial role in regulating the ubiquitin system as well as the processes in which it is involved, including cell signalling, intracellular trafficking, cell cycle progression, and immune response[72,76,77]. Altered regulation of ubiquitination is involved in the pathogenesis of many diseases including viral infection and some cancers, and as a result, DUBs have become a potential target for drugs[77,78].

The ovarian tumor proteases are one of five families of DUBs. This family shares a similar active site structure known as the ovarian tumor domain (OTU). Ovarian tumor proteases are cysteine proteases that contain a conserved catalytic triad, including a cysteine residue responsible for cleaving the isopeptide bond to release free ubiquitin. The OTU domain active site is somewhat similar to those of the papain family of plant cysteine proteases, whose catalytic mechanism has been described in detail[72,79]. Interestingly, the crystal structure of at least one OTU catalytic domain reveals a catalytic triad that is in a catalytically inactive conformation, suggesting that some conformational change might be necessary for catalysis[80]. Many human and animal viruses, such as the crimean-congo haemorrhagic fever virus, produce proteins that contain OTU domains capable of deubiquitinating a broad spectrum of substrates in mammalian

cells[81,82]. Ubiquitin signalling is an important process in innate immunity, and it has been shown that deubiquitination functions to help the virus avoid an antiviral response from the host[82,83].

1.4. OTU1

We have studied the dynamics of an OTU domain-containing deubiquitinase named Otu1 from the yeast *Saccharomyces cerevisiae*. Otu1 has been shown to be involved in the endoplasmic reticulum (ER)-associated degradation pathway by interaction with Cdc48, a chaperone-like AAA ATPase[84]. Cdc48 is involved in escorting polyubiquitinated proteins to the proteasome for degradation[84]. Among other partners, Otu1 is known to directly interact with Cdc48, suggesting that it may participate in regulating protein degradation in the ER[84,85]. Otu1 preferentially cleaves Lys48-linked polyubiquitin chains[84,85]. The Otu1 structure consists of three domains: An N-terminal ubiquitin-like fold (UBX) domain, an OTU catalytic domain, and a C-terminal putative zinc-binding Cys_2His_2 (C_2H_2) domain[84,85]. The UBX domain facilitates Otu1's interaction with Cdc48 but its removal has no effect on the enzyme's deubiquitinating activity[84,85]. A crystal structure of the catalytic domain of Otu1 has been solved in complex with ubiquitin[85]. The crystallized construct lacked the UBX domain, and the putative zinc-binding domain was present but was invisible in the electron density map, possibly due to disorder[85]. Interestingly, the structure of the catalytic domain contains a short loop of amino acids covering the active site where the proteolytic reaction takes place, apparently blocking access to substrate[85,86]. This loop appears to be highly conserved among OTU domains, including those of viruses[86]. Some DUBs from other families also have active-site-blocking loops which are believed to be involved in regulation of their activity[31].

Since Otu1 is functionally active in vitro[85], we believe it must be able to change its conformation and open up the loop to allow substrate binding and catalysis. If true, this would make Otu1 an ideal model to study enzyme conformational dynamics both for its biological significance as well as for a better understanding of enzyme function in general. Our long-term goal is to develop a model that completely describes the dynamic changes that occur during the Otu1 reaction cycle. However, we must first understand the dynamics of the free enzyme. The scope of this project encompasses probing the dynamics of the active site. We hypothesize that free Otu1 exists in equilibrium between a conformation capable of binding substrate (open loop) and a conformation incapable of binding substrate (closed loop). Thus, the initial step is to establish whether such a conformational change can be detected in solution. We have combined rapid mixing by stopped-flow with intrinsic fluorescence and UV-Vis spectroscopy to study the reaction of the Otu1 active site with 4,4'-Dithiodipyridine (DTDP), a cysteine-reactive probe. Our results suggest that the OTU domain active site undergoes a conformational change as a rate-limiting step during the reaction.

2. Materials and Methods

2.1. REAGENTS

Growth media were purchased from Becton Dickinson. Acetic acid, Glycerol, tris(hydroxymethyl)aminomethane (TRIS), sodium chloride, dithiothreitol (DTT), hydrochloric acid, sodium hydroxide, imidazole, methanol, sodium dodecyl sulfate (SDS), sodium acetate, ethidium bromide, kanamycin, glycine, acrylamide, boric acid, and sodium carbonate were purchased from Fisher Scientific. Sodium borate was purchased from Mallinckrodt. Ethylenediaminetetraacetic acid (EDTA), dibasic sodium phosphate, monobasic sodium phosphate, bis-tris-propane, 4,4'-dithiodipyridine (DTDP or aldrithiol-4), and N-acetylcysteine amide (NACA) were purchased from Sigma-Aldrich. Isopropyl β-D-1-thiogalactopyranoside (IPTG), dNTPs, and agarose were purchased from Invitrogen.

2.2. PREPARATION OF OTU1ΔUBX

2.2.1. PREPARATION OF OTU1ΔUBX EXPRESSION CONSTRUCT

The Otu1 enzyme from *Saccharomyces cerevisiae* consists of three domains: An N-terminal ubiquitin-like (UBX) domain, an OTU catalytic domain, and a C-terminal putative zinc-binding domain[84,85]. Removal of the UBX domain (amino acids 1-86) has been shown to have no effect on the deubiquitinating activity of Otu1[84,85]. The remainder of Otu1 (amino acids 91-301), cloned into the NdeI and BamH1 sites of a modified version of pET28b(+) (kan^R) (Novagen) (with a reduced multiple cloning site composed only of NdeI/SpeI/BamH1) and transformed into *E. coli* strain BL21-Gold (DE3) (New England Biolabs), was graciously provided by Dr. Brian Mark (Department of Microbiology, Faculty of Science, University of Manitoba). This construct, named Otu1ΔUBX, incorporated a 6xHis tag at the C-terminus of the enzyme followed by a

translation stop codon. The 6xHis tag was included for affinity purification of the enzyme. This construct was previously published in James *et al.*[81].

This plasmid was isolated, using a commercial plasmid-prep kit (QIAGEN), from an overnight culture of cells grown in LB media supplemented with 35 µg/mL kanamycin at 37ºC (LB kan^{35}). The construct was transformed into *E. coli* strain BL21-Gold (DE3) made competent by the chemical method, and transformants were selected on LB agar kan^{35}. A positive transformant colony was frozen at -80 °C in LB media containing 20% glycerol to be used to start all future cultures for overexpression. The Otu1ΔUBX construct was sequenced. Sequencing was performed by The Centre for Applied Genomics, The Hospital for Sick Children, Toronto, Canada, using in-house T7 primers: T7: 5'-TAATACGACTCACTATAGGG-3', T7term: 5'-GCTAGTTATTGCTCAGCGG-3'.

2.2.2. OVEREXPRESSION OF OTU1ΔUBX

An overnight culture of *E. coli* BL21 containing Otu1ΔUBX expression construct was used to inoculate one or more 2 L baffled flasks each containing 500 mL LB kan^{35}. The culture was grown at 37 °C with 190 rpm shaking to an OD_{600nm} of around 0.4-0.8. Expression of enzyme was induced by the addition of Isopropyl β-D-1-thiogalactopyranoside (IPTG) to 1 mM, and the culture was incubated overnight at 16 °C with 190 rpm shaking. The culture was pelleted by centrifugation at 6000 rpm for 20 minutes at 4 °C (Sorvall SLA-3000 rotor). The cell pellet was either used immediately for protein purification or was frozen at -80 °C until use.

In *E. coli* BL21 (DE3), the constitutively expressed lac repressor protein (LacI) binds to the lac operator sequence in front of both T7 polymerase on the chromosome as well as the cloned gene on the pET vector (in this case, Otu1ΔUBX), preventing their expression[87]. When IPTG (an indigestible lactose analog) is provided to the cell, it binds to LacI and lifts repression. This

results in expression of T7 polymerase, which in turn transcribes Otu1ΔUBX on the pET vector through the T7 promoter sequence. This process allows for tight control of gene expression on the vector.

2.2.3. PURIFICATION OF OTU1ΔUBX

Two or three cell pellets were resuspended in up to approximately 20 mL of lysis buffer [50 mM TRIS, 300 mM NaCl, 1-2mM DTT, pH 8.0], and lysed using a French pressure cell press (AMECO), which included ~5 passes at 1000 psi. The crude lysate was centrifuged at 12000 rpm for 1 hour at 4 ºC (Sorvall SS-34 rotor), and the pellet was discarded.

All chromatography steps were carried out on an AKTA FPLC (GE Healthcare) at 4 °C. Clear lysate was passed through 3 mL bed volume of Ni-NTA resin (QIAGEN) pre-equilibrated in lysis buffer. In the FPLC program, the column was rinsed with ten column volumes of lysis buffer, followed by ten column volumes of the same buffer containing 12.5 mM imidazole, ten column volumes of buffer containing 25 mM imidazole, and finally the his-tagged protein was eluted in buffer containing 250 mM imidazole. Protein-containing fractions in the eluate were assessed by absorbance at 280 nm, pooled, and dialyzed at 4 °C overnight against 1 L of dialysis buffer [25 mM TRIS, 150 mM NaCl, 2 mM DTT, pH 8.0] using Spectra/Por 7 pre-treated dialysis membrane with 2 kDa pore size (Spectrum Labs).

The dialyzed sample was concentrated to ~2 mL using an Amicon Ultra centrifugal filter (Millipore) with 10 kDa molecular weight cut-off (mwco). The solution was applied to a Superdex 75 column (GE Healthcare) pre-equilibrated in buffer containing [25 mM TRIS, 150 mM NaCl, 1 mM DTT, pH 8.0]. This column separates proteins based on size and therefore further purified the protein sample. The fractions corresponding to the single largest peak of eluted protein were combined (assessed by absorbance at 280 nm, usually at ~75 mL elution

volume). The purified enzyme sample was divided into aliquots of 50 or 100 µL and frozen at -80 °C until use. The concentration of the purified protein sample was measured by absorbance at 280 nm using an extinction coefficient of 19940 M^{-1} cm^{-1}. The extinction coefficient was determined theoretically using the online ExPASy Protparam tool[88,89]. Protein purity was assessed by SDS-PAGE: samples were diluted in 2x loading buffer, heated at 98°C for 10 minutes, and loaded onto a 12% acrylamide SDS-polyacrylamide gel. Broad-range SDS-PAGE molecular weight standards (Bio-rad) was used as standards ladder. Electrophoresis proceeded in Tris-glycine-SDS buffer, and protein bands were visualized by staining with brilliant blue R-250 (Fisher).

2.3. PREPARATION OF OTU1ΔUBXΔZN

2.3.1. PREPARATION OF OTU1ΔUBXΔZN EXPRESSION CONSTRUCT

C-terminal to its catalytic domain, Otu1 contains a putative zinc-binding domain[85] (residues 264-301). To generate a truncated enzyme lacking the putative zinc-binding domain, a PCR method of site-directed mutagenesis[90] was employed, using the above Otu1ΔUBX expression plasmid construct as a template. The forward primer [5'-CACCACCACTAACTCGAGCACCA-3', from Integrated DNA technologies, 5'phosphorylated] was designed to start at the Gly-Ser linker at the beginning of the C-terminal 6xHis tag and amplify around the entire plasmid. The reverse primer [5'-GTGGTGGTGGGATCCGAAGGAATAGCCAGTTTGCTTCAAATTTGA-3', from Integrated DNA technologies, 5'phosphoryated] was designed to start at residue 174 of Otu1ΔUBX (residue 263 of full-length Otu1) (where the catalytic domain ends and after which the putative zinc-binding domain begins) and amplify *backwards* around the plasmid. Thus, by this method, the entire plasmid is amplified excluding the putative zinc-binding domain. The "Around-the-horn" PCR was performed using Phusion high-fidelity DNA polymerase (New

England Biolabs) in HF buffer (New England Biolabs) along with 2 µM of each dNTP and 0.5 µM of each primer. The PCR program involved a 90 second initial denaturation at 98 °C, followed by a three-part cycle of: 10 seconds at 98 °C, 20 seconds at 63 °C, and 210 seconds at 72 °C. The three-part cycle was repeated thirty times, and the program ended with a 10-minute incubation at 72 °C. The entire completed reaction mixture was separated on a 1.1% agarose TAE gel, visualized using ethidium bromide, and the band corresponding to the roughly 6 kb PCR product was purified using a commercial QIAquick Gel Extraction Kit (QIAGEN).

The two PCR primers were phosphorylated at the 5' ends. This allowed the two ends of the PCR product to be connected by a simple ligation reaction after gel-extraction, resulting in a circularized plasmid. The ligation reaction used Instant Sticky-end Ligase Master Mix (New England Biolabs) and was allowed to proceed for 15 minutes at room temperature. The ligation product was transformed into *E. coli* DH5α cells (New England Biolabs) made competent by the chemical method. Transformation was done using heat shock method, which involved incubation at 1 °C for 30 minutes, followed by 42 °C for 90 seconds, and finally in LB media at 37 °C for 1 hour. Positive transformants were selected for on LB agar (kan^{35}) plates. Putative transformants were screened by PCR. This construct was named "Otu1ΔUBXΔZN", because it lacks both the UBX domain and the putative zinc-binding domain. To ensure the success of this method, the final plasmid product was sequenced. Sequencing was performed by The Centre for Applied Genomics, The Hospital for Sick Children, Toronto, Canada, using in-house T7 primers: T7: 5'-TAATACGACTCACTATAGGG-3', T7term: 5'-GCTAGTTATTGCTCAGCGG-3'.

The Otu1ΔUBXΔZN expression plasmid construct was transformed into *E. coli* BL21-gold (DE3) for protein overexpression. As above, a sample of culture was stored in LB media

containing 20% glycerol at -80 °C which was used to start all subsequent overnight cultures of this construct.

2.3.2. OVEREXPRESSION OF OTU1ΔUBXΔZN

Overexpression of Otu1ΔUBXΔZN followed the same procedure as with Otu1ΔUBX.

2.3.3. PURIFICATION OF OTU1ΔUBXΔZN

Purification of Otu1ΔUBXΔZN followed the same procedure as with Otu1ΔUBX, with one important change: the superdex 75 column was instead equilibrated in buffer *lacking* DTT [25 mM TRIS, 150 mM NaCl, pH 8.0]. This change resulted in the removal of DTT from the sample during chromatography, as small molecules (such as DTT in the enzyme sample) are trapped in the column for longer than the much larger proteins. Thus, enzyme molecules leave the superdex 75 column in the equilibration buffer above.

2.4. DATA ANALYSIS

All data analysis was carried out using SigmaPlot 12 software (Point Richmond, CA) unless otherwise indicated.

2.5. DEUBIQUITINASE ACTIVITY ASSAY

Deubiquitinating activity of the recombinant enzymes was measured using a procedure adapted from the literature[85,91]. In short, the cleavage of 250 nM Ubiquitin-AMC (Ub-AMC) (BostonBiochem) was catalyzed by the addition of 50 nM purified enzyme (Otu1ΔUBX or Otu1ΔUBXΔZN) in [50 mM TRIS, 50 mM NaCl, 2 mM DTT, pH 7.5) at room temperature, and the increase in fluorescence at 460 nm was monitored for one hour, using a Jobin-Yvon Fluorolog fluorescence spectrophotometer (Horiba) with 360 nm excitation light and 1 nm emission and excitation slits, and in a 10 mm by 3.5 mm quartz cuvette (Starna Cells). The

average fluorescence intensity of the Ub-AMC solution prior to addition of enzyme was subtracted from each data point.

It has been suggested that the cleavage of Ub-AMC catalyzed by Otu1 or Otu1ΔUBX follows Michaelis-Menten kinetics[85]. The Michaelis-Menten expression for the rate of an enzyme-catalyzed reaction is shown in equation (2-1)[16].

$$reaction\ rate = \frac{d[P]}{dt} = \frac{k_{cat}[E][S]}{K_M + [S]} \quad (2\text{-}1)$$

Where "[P]" equals the concentration of products at time "t", "[E]" equals the concentration of enzyme, "[S]" equals the concentration of substrate at time "t", and "$\frac{k_{cat}}{K_M}$" equals the Michaelis-Menten specificity constant. At substrate concentrations much lower than K_M, equation (2-1) can be approximated to equation (2-2).

$$\frac{d[P]}{dt} = \frac{k_{cat}}{K_M}[E][S] \quad (2\text{-}2)$$

Integration of equation (2-2) results in equation (2-3).

$$[P] = [P]_\infty \left(1 - e^{-\frac{k_{cat}}{K_M}[E]t}\right) = [P]_\infty (1 - e^{-kt}) \quad (2\text{-}3)$$

Where "$[P]_\infty$" equals the concentration of products after infinite time. Because the evolved fluorescence at 460 nm is proportional to the product concentration, the time course of product formation follows an exponential rise to maximum as described by:

$$F - F_0 = F_\infty (1 - e^{-kt}) \quad (2\text{-}4)$$

Where "F" equals the fluorescence intensity at time "t", "F_0" equals the background fluorescence intensity, "F_∞" equals the change in fluorescence intensity after time equals infinity, and "k" equals the apparent rate constant for the rise, which will be equal to $\frac{k_{cat}}{K_M}[E]$. Therefore, the

measured fluorescence time course was fit to equation (2-4) and the fitted value of "k" was used to calculate $\frac{k_{cat}}{K_M}$. This was repeated at least four times for each enzyme.

2.6. DIFFERENTIAL SCANNING CALORIMETRY (DSC)

Enzyme samples were dialyzed at 4 °C overnight against 1 L of buffer [19 mM Na_2HPO_4, 31 mM NaH_2PO_4, adjusted to pH 7.0] using commercial Spectra/Por 7 pre-treated dialysis membrane with 2 kDa pore size (Spectrum Labs). The dialysate was used as the reference solution, so that the presence of enzyme accounts for the only difference between enzyme and reference solutions. Concentration of the enzyme samples was measured after dialysis by absorbance at 280 nm using an extinction coefficient of 19940 M^{-1} cm^{-1} (58 μM Otu1ΔUBX or 97 μM Otu1ΔUBXΔZN). All dialyzed enzyme and buffer solutions were degassed for 10 minutes prior to DSC. DSC experiments were performed using a Nano DSC (TA Instruments) with 0.3 mL capillary cell volume. Samples were equilibrated at 20 °C and then heated to 95 °C with a scan rate of 1 °C per minute and at 3 atm. Data were analyzed using NanoAnalyze (TA Instruments), and the baseline subtracted heat rate was fit to a two-state scaled model for the transition. The melting temperature (T_m) is the peak of the melting curve.

2.7. UV-VIS ABSORBANCE SPECTROSCOPY

Absorbance measurements were carried out on a Helios Zeta UV-Vis spectrophotometer (Thermo Scientific), using 10 mm by 3.5 mm quartz cuvettes (Starna Cells).

2.8. STEADY-STATE FLUORESCENCE SPECTROSCOPY

All fluorescence spectra were recorded on a Jobin-Yvon Fluorolog fluorescence spectrophotometer (Horiba), using 10 mm by 3.5 mm quartz cuvettes (Starna Cells). The fluorescence emission spectrum of 2 μM Otu1ΔUBXΔZN was collected from 300 nm to 500 nm,

using 280 nm excitation light and 2.25 nm emission and excitation slits, at room temperature and in different buffer pH conditions from pH 7 to 10: 100 mM Na_2HPO_4, 0.5 mM EDTA, pH 7.0; 100 mM Na_2HPO_4, 0.5 mM EDTA, pH 7.5; 100 mM TRIS, 0.5 mM EDTA, pH 8.0; 100 mM TRIS, 0.5 mM EDTA, pH 8.5; 100 mM TRIS, 0.5 mM EDTA, pH 9.0; 100 mM Na_2CO_3, 0.5 mM EDTA, pH 9.5; 100 mM Na_2CO_3, 0.5 mM EDTA, pH 10.0. Data analysis was carried out in SigmaPlot 12.3. A reference spectrum was collected for each buffer solution without enzyme and subtracted.

2.9. CIRCULAR DICHROISM (CD) SPECTROSCOPY

All CD spectra were recorded using a J-810 spectropolarimeter (JASCO) with a 0.05 cm cylindrical cuvette. The CD spectrum of 5 μM Otu1ΔUBXΔZN in buffer containing [4 mM Na_2HPO_4, 6 mM NaH_2PO_4, 0.4 mM $Na_2B_4O_7$, 5 mM H_3BO_3, pH 7.0] was collected from 185 nm to 260 nm at room temperature, using a 20 nm/min scan rate, 2 second response time, and 0.1 nm data pitch. The above solution was titrated with a solution of 5 μM Otu1ΔUBXΔZN in buffer containing [4 mM Na_2HPO_4, 6 mM NaH_2PO_4, 10 mM $Na_2B_4O_7$, adjusted to pH 10.0], and five additional spectra were recorded during the process. At each point, the pH was measured. This was repeated for the same buffers containing no enzyme to obtain a blank spectrum at each point. For each pH, a blank spectrum was subtracted from the enzyme spectrum.

2.10. THIOL-REACTIVE PROBES

5,5'dithio-bis(2-nitrobenzoic acid) (DTNB), also known as Ellman's reagent, is a small molecule whose absorbance spectrum changes upon reaction with compounds containing thiol groups, such as that of the amino acid cysteine[92,93]. Specifically, the product of such a reaction, 5-thio-2-nitrobenzoic acid (TNB), absorbs strongly at 412 nm (ε_{412} = 14150 M^{-1} cm^{-1})[92]. For this reason, it has been commonly used as a probe for spectroscopic assays, such as the quantification of

protein thiol groups[92,93]. DTNB is charged in solution at neutral pH and it has been shown to react incompletely with thiols[94]. 4,4'-dithiodipyridine (DTDP), also known as Aldrithiol-4 or 4-PDS, is a smaller compound that reacts more quickly and completely with thiol residues than DTNB, and is mostly uncharged in solution at neutral pH[94]. DTDP reacts with reduced thiols to form a conjugated product as well as a free 4-thiopyridone (4-TP) molecule (Figure 2-1)[94-96]. The absorbance spectrum of the free 4-TP product contains a peak at 324 nm (ε_{324} = 21400 M^{-1} cm^{-1}) which is not present in the spectrum of DTDP[94]. Thus, reaction of DTDP with a reduced thiol group such as in cysteine can be followed by measuring the increase in absorbance at 324 nm over time.

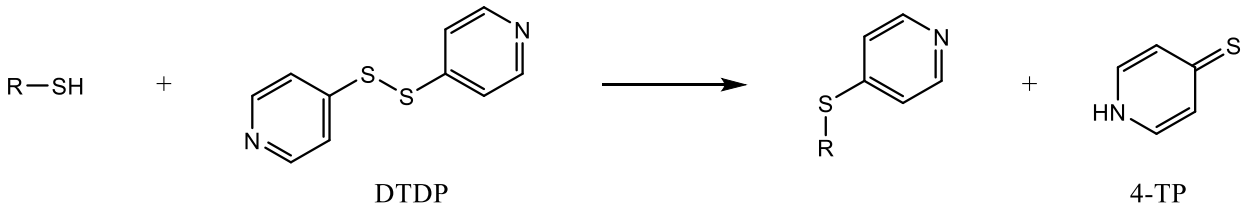

Figure 2-1: Scheme for the reaction of a thiol-containing molecule (RSH) with DTDP, yielding a disulfide and 4-TP.

2.10.1. PREPARATION OF THIOL-REACTIVE PROBES

DTDP powder was dissolved up to about 150-200 mM in approximately 0.4 M HCl, and either used immediately or frozen at -20 °C until use. Prior to use, this stock was diluted in the desired buffer (at least 15 fold), and the pH was readjusted with NaOH. The concentration of DTDP in solution was determined by absorbance at 246 nm (ε_{247} = 1.63x10^4 M^{-1} cm^{-1})[96]. The highest attainable concentration of DTDP above pH 7.0 was about 10 mM (significant turbidity or precipitation was observed over 10 mM). As stopped-flow mixes two reactant solutions in equal amounts, the maximum attainable concentration of DTDP in reaction was 5 mM.

2.11. STOPPED-FLOW SPECTROPHOTOMETRY

In essence, a stopped-flow spectrophotometer is analogous to any other absorbance or fluorescence spectrophotometer, except that it allows for very fast mixing of two solutions. A simplified schematic of a stopped-flow instrument is shown in Figure 2-2. The two solutions to be mixed are placed in separate drive syringes (red and green in Figure 2-2). The syringes are connected by tubing to a T-mixer, where the solutions are mixed, followed by an optical cell for spectroscopic measurement of the mixture and finally a stop syringe. A drive ram, often powered by compressed gas, simultaneously compresses both sample syringes, pushing sample through the system and filling the stop syringe. Flow must stop when the stop syringe is full, at which point spectroscopic observation of the mixture in the optical cell is begun. The process is very fast, such that the reaction in the optical cell can be monitored within 1-2 ms of mixing[56]. The progress of the reaction can then be measured spectroscopically for up to minutes after[56].

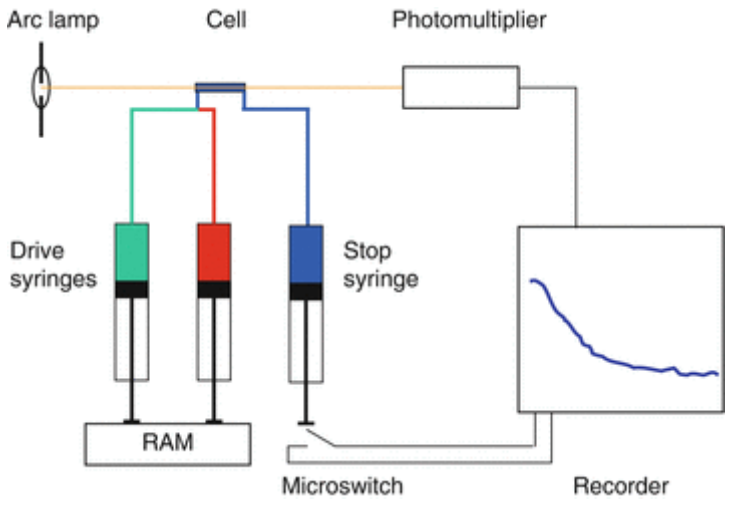

Figure 2-2: Schematic diagram of the key components of a stopped-flow spectrophotometer. (Springer Encyclopedia of Biophysics, Stopped-Flow Techniques, 2013, pp 2460-2466, Clive R. Bagshaw, Copyright European Biophysical Societies' Association (EBSA) 2013, used with permission of Springer.)

2.11.1. MEASUREMENT OF REACTION KINETICS

All stopped-flow reactions were carried out using an SX20 Stopped Flow Spectrometer (Applied Photophysics). For each reaction, both reactants were diluted into the same buffer. Otu1ΔUBXΔZN or NACA solution was placed into one drive syringe, while DTDP solution was placed into the other drive syringe. The SX20 injected equal volumes of the two solutions into the optical cell and over time recorded either the absorbance at 324 nm, or the fluorescence intensity through a 320 nm longpass filter at an excitation wavelength of 280 nm. In the case of fluorescence, the excitation slits and the PMT voltage were optimized for each reaction. In order to obtain pseudo first-order kinetics, the concentrations of DTDP were always kept in at least 5-fold excess of Otu1ΔUBXΔZN or NACA. NACA concentrations were 10-150 μM, Otu1ΔUBXΔZN concentrations were 2 uM for fluorescence or 20 uM for absorbance. The dead time (mixing time) of the instrument was assumed to be 1 millisecond; therefore data collected faster than 1 millisecond were excluded. Reactions were repeated several times (usually 2-20) and an average trace was obtained.

Reactions of 10-150 μM NACA with DTDP were carried out at 12.5 °C, and an increase in absorbance at 324 nm was recorded. Reactions of 2 μM Otu1ΔUBXΔZN with DTDP were carried out at 12.5 °C, and a decrease in fluorescence intensity was recorded at 280 nm excitation light. In this report, all concentrations listed for materials used in stopped-flow refer to the concentration after solutions were mixed (reaction concentration). Between five and thirty replicates were recorded for each trace and averaged.

3. Results

In this work, we have studied the properties of the active site of the Otu1 enzyme. We have overexpressed and purified the Otu1 catalytic domain and compared its biophysical properties with those of the intact protein. We have also probed the catalytic domain using the cysteine-labelling molecules DTDP. The labelling reaction kinetics of the catalytic cysteine with DTDP have been followed using stopped-flow spectroscopy methods. The results of this study have enabled us to determine the dynamic properties of the active site of this enzyme.

3.1. TRUNCATION OF OTU1ΔUBX

C-terminal to its catalytic domain, Otu1 contains a putative C_2H_2 zinc-binding domain[85] (residues 264-301). When Otu1ΔUBX in complex with ubiquitin was crystallized by Messick *et al*, the C_2H_2 domain was not visible in the electron density map[85]. This domain contains two cysteine residues which would potentially react with the cysteine-labelling probe DTDP. This will complicate the kinetic analysis of the reaction of this probe. Therefore, standard molecular biology techniques were employed to remove the putative zinc-binding domain. The resulting construct, Otu1ΔUBXΔZN, comprises simply the catalytic OTU domain that contains only a sole cysteine in the active site as well as a C-terminal 6x-His tag. Genetic sequence analysis of the expression plasmid containing this construct confirmed the success of the cloning methods. Figure 3-1 shows SDS-PAGE analysis of Otu1ΔUBX and the purified Otu1ΔUBXΔZN. The absence of any other band in the Otu1ΔUBX or Otu1ΔUBXΔZN lanes suggests that no significant contaminants exist in the purified protein samples. The relative position of each protein band indicates that the two species differ by a molecular mass of approximately 4-5 kDa. This shows that the 38 residues of Otu1ΔUBX that form the putative C_2H_2 domain of this protein have been successfully removed and that we have isolated the catalytic domain of Otu1.

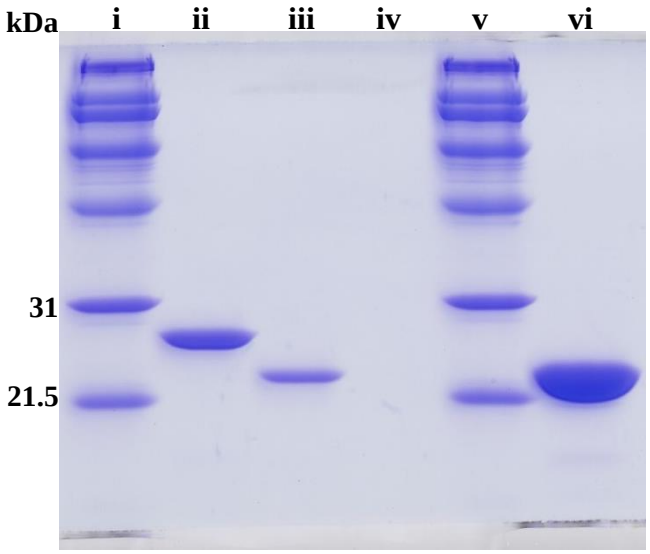

Figure 3-1: SDS-PAGE of purified protein samples. (i) Molecular weight standards (Bio-rad broad range); (ii) 2.5 µg purified Otu1ΔUBX; (iii) 2.5 µg purified Otu1ΔUBXΔZN; (v) molecular weight standards; (vi) 7 µg purified Otu1ΔUBXΔZN. Samples run on 12% acrylamide gel and visualized by coomassie staining.

3.2. DEUBIQUITINASE ACTIVITY OF PURIFIED ENZYMES

Figure 3-2 shows the progress curve of the action of Otu1ΔUBXΔZN on the substrate Ub-AMC. It can be observed that the addition of the enzyme leads to an increase in fluorescence intensity measured at 460 nm; this increase results from the catalytic cleavage of the AMC moiety from ubiquitin. Based on the literature[85], a concentration of 0.25 µM Ub-AMC is in the low-concentration regime, such that the approximation in equation (2-2) is valid. In Table 3-1, the specificity constant for the two enzymes Otu1ΔUBXΔZN and Otu1ΔUBX are reported for comparison. These values demonstrate: A) the specificity constant obtained for Otu1ΔUBX is consistent with the reported values in the literature[85]; B) the truncation has had no significant effect on the activity of the enzyme.

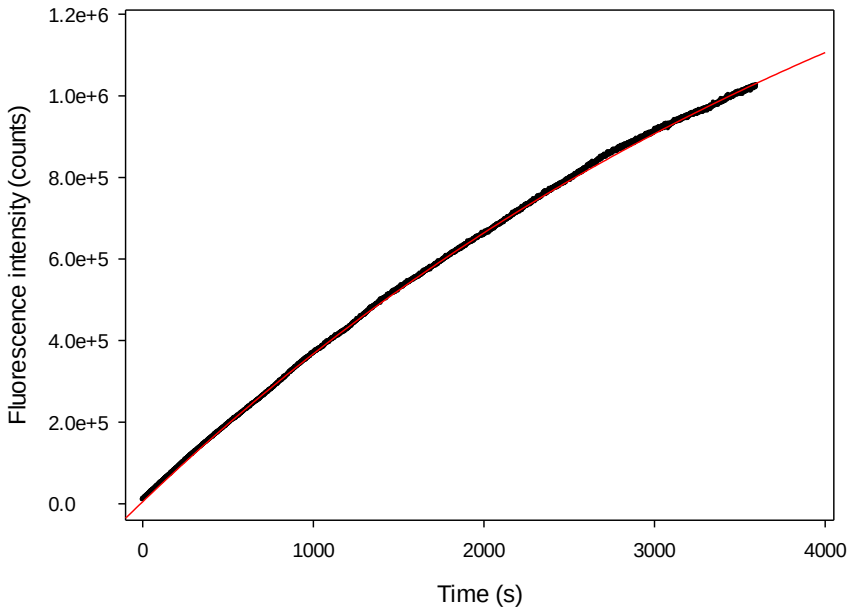

Figure 3-2: Deubiquitinating activity of Otu1ΔUBXΔZN. The cleavage of 250 nM Ub-AMC was catalyzed by the addition of 50 nM Otu1ΔUBXΔZN, and the increase in fluorescence emission at 460 nm (with 360 nm excitation light) was recorded over time. The reaction was performed at room temperature, buffered using 50 mM TRIS, 50 mM NaCl, 2 mM DTT, and adjusted to pH 7.5. The red line represents the best fit to a mono-exponential rise to maximum, as given by equation (2-4).

Table 3-1: Specificity constant of purified recombinant deubiquitinases. Cleavage of Ub-AMC catalyzed by each DUB was monitored by fluorescence, and the progress curve was fit to equation (2-4) to obtain the specificity constant. At least four trials were performed for each enzyme, and the average ± the standard deviation is presented in the table.

Enzyme	k_{cat}/K_M (M^{-1} s^{-1})
Otu1ΔUBX	4600 ± 900
Otu1ΔUBXΔZN	5000 ± 2000

3.3. DIFFERENTIAL SCANNING CALORIMETRY OF PURIFIED ENZYMES

Figure 3-3 shows melting curves for Otu1ΔUBX and Otu1ΔUBXΔZN obtained by DSC. It can be seen that the thermal transition midpoint, or melting temperature (T_m), of the two enzymes differs by less than 2 °C. This indicates that removal of the putative C_2H_2 domain has had only a

minor effect on the thermal stability of the enzyme. Therefore, it is likely that minimal interactions exist between the catalytic OTU domain and the putative zinc-binding domain.

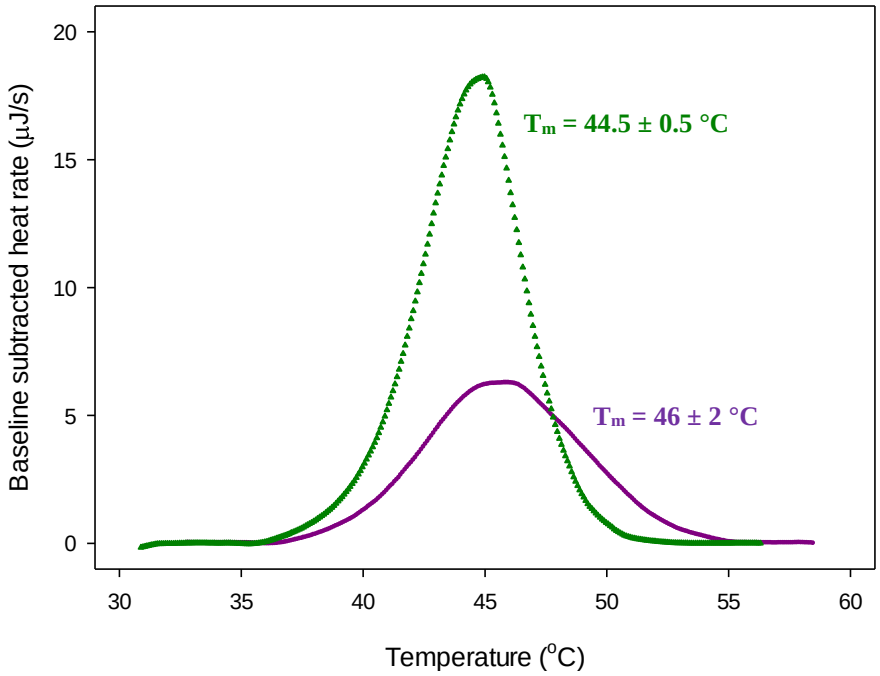

Figure 3-3: Thermal unfolding of recombinant enzymes monitored by DSC. 58 μM Otu1ΔUBX (purple) or 97 μM Otu1ΔUBXΔZN (dark green) in 50 mM phosphate buffer at pH 7 was heated from 20 °C to 95 °C at 1 °C per minute and at 3 atm using DSC. The T_m is the peak of the melting curve, as determined by the best fit to a two-state scaled model for the transition.

3.4. EFFECT OF PH ON OTU1ΔUBXΔZN STRUCTURE

We have investigated the effect of pH on the structure of Otu1ΔUBXΔZN using fluorescence and circular dichroism spectroscopies. The fluorescence emission of the indole ring of tryptophan is sensitive to local solvent polarity and this property can be used to detect structural perturbations[61]. Otu1ΔUBX contains two tryptophan residues, Trp168 and Trp175[85]. The existence of two tryptophan residues may complicate the interpretation of our fluorescence data. Figure 3-4 depicts the fluorescence emission spectra of Otu1 over a range of buffer pH conditions. The fluorescence emission peak undergoes a blue shift of 6 nm over the pH range.

The fact that a blue shift is observed indicates that the fluorescing tryptophan residue has become slightly less exposed to solvent[61]. This observation is consistent with a minimal change in the protein tertiary structure.

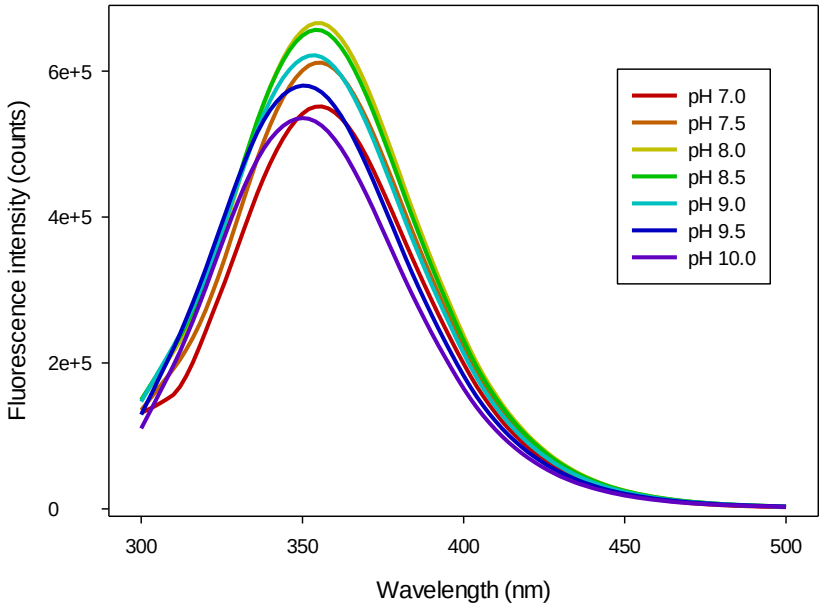

Figure 3-4: Fluorescence emission spectrum of Otu1ΔUBXΔZN measured under different buffer pH conditions. The emission spectrum of 2 μM Otu1ΔUBXΔZN in different buffers was collected at room temperature using 280 nm excitation light. See methods section for composition of each buffer.

The pH-induced perturbations in the secondary structure of Otu1ΔUBXΔZN have been monitored using CD spectroscopy. The CD spectra of Otu1ΔUBXΔZN under multiple pH conditions from pH 7.00 to pH 9.73 are shown in Figure 3-5. Regions corresponding to beta sheet and alpha helix are only slightly changed over the pH range, while no significant increase in random coil is observed. We therefore conclude that the enzyme secondary structure is minimally perturbed across the entire pH range.

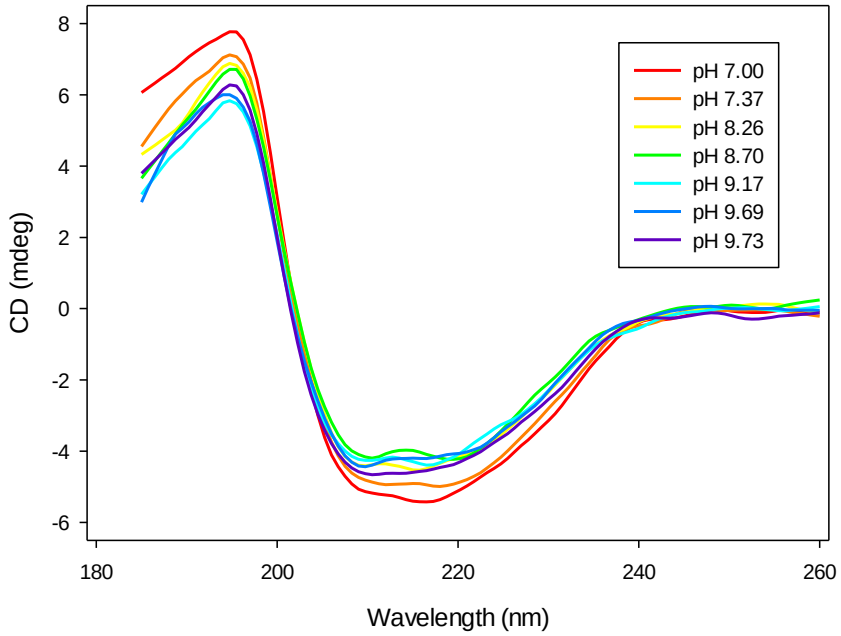

Figure 3-5: Circular dichroism spectrum of Otu1ΔUBXΔZN measured under different buffer pH conditions. 5 µM Otu1ΔUBXΔZN in buffer at pH 7.0 was titrated with 5 µM Otu1ΔUBXΔZN in buffer at pH 10, and the CD spectrum was obtained at room temperature at several points during the process. See Methods section for details and buffer composition.

3.5. REACTION KINETICS OF NACA WITH DTDP

Complete analysis of the reaction kinetics of DTDP with the active-site cysteine of Otu1 requires knowledge of the reaction rate of DTDP with a fully-accessible cysteine. N-acetylcysteine amide (NACA) has been chosen as model for free cysteine in a peptide, and the kinetics of its reaction with DTDP have been studied using stopped-flow. Figure 3-6 shows example traces of the reaction of NACA with three different concentrations of DTDP. It can be observed that the rapid mixing of DTDP with NACA results in an increase in absorbance at 324 nm, which results from the production of the product molecule 4-thiopyridine. The time course of each reaction follows an exponential rise to maximum as given by equation (3-1):

$$A - A_0 = A_\infty\left(1 - e^{-k_{app}t}\right) \qquad (\ 3\text{-}1\ )$$

Where “A” equals the absorbance at 324 nm at time “t”, “A_0” equals the background absorbance at 324 nm, “A_∞” equals the change in absorbance at 324 nm after time equals infinity, and “k_{app}” equals the rate constant for the rise. This equation can be rearranged into equation (3-2):

$$A = y_0 + a\left(1 - e^{-k_{app}t}\right) \qquad (3\text{-}2)$$

Where “y_0” is equal to A_0, and “a” is equal to A_∞.

Figure 3-6 depicts typical progress curves of the reaction of NACA with three different concentrations of DTDP. These data indicate that k_{app} may exhibit a possible DTDP concentration dependence. In addition, as can be seen in Figure 3-7, reacting NACA with the same amount of DTDP shows that k_{app} may also depend on the pH of the solution. In order to investigate these dependencies, progress curves of the reaction of NACA with a range of DTDP concentrations have been collected under several different buffer pH conditions. Each reaction progress curve was fit to equation (3-2), and the results are tabulated in Table 3-2. In Figure 3-8, the apparent rate constant k_{app} is plotted as a function of DTDP concentration for each buffer pH condition. Clearly, at each given pH, k_{app} is linearly dependent on DTDP concentration. The results of these linear fits are tabulated in Table 3-3. In addition, a close examination of the parameter “a” indicates that the slopes obtained from the linear regression exhibit a strong pH dependence.

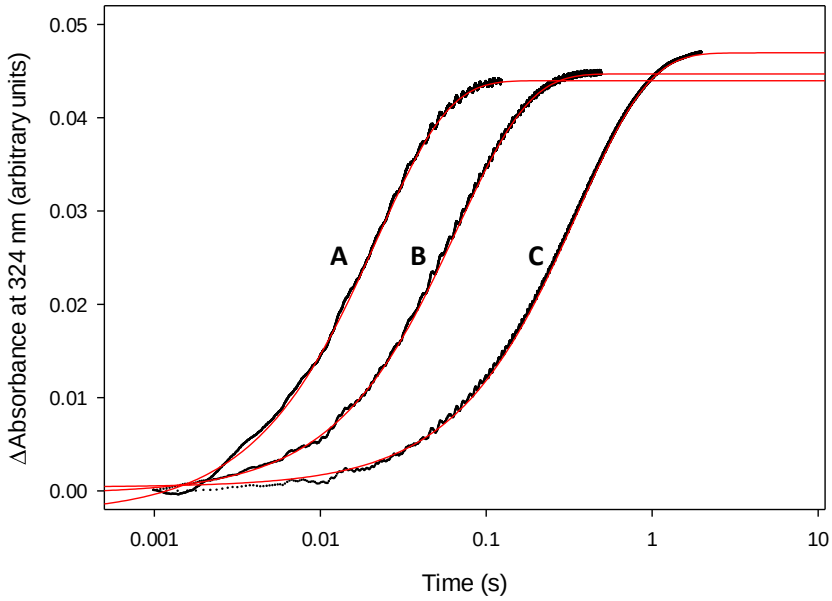

Figure 3-6: Stopped-flow traces reported as changes in absorbance monitored at 324 nm as a function of time due to reaction of 20 µM NACA with DTDP (black dots). The different traces represent different DTDP concentration values. The reactions were performed under pseudo-first-order conditions at 12.5 °C buffered using 100 mM TRIS, 0.5 mM EDTA, at pH 8.5. The traces represent: A = 3160 µM DTDP, B = 1000 µM DTDP, C = 200 µM DTDP. The red lines represent the best fit to a mono-exponential rise to maximum, as given by equation (3-2).

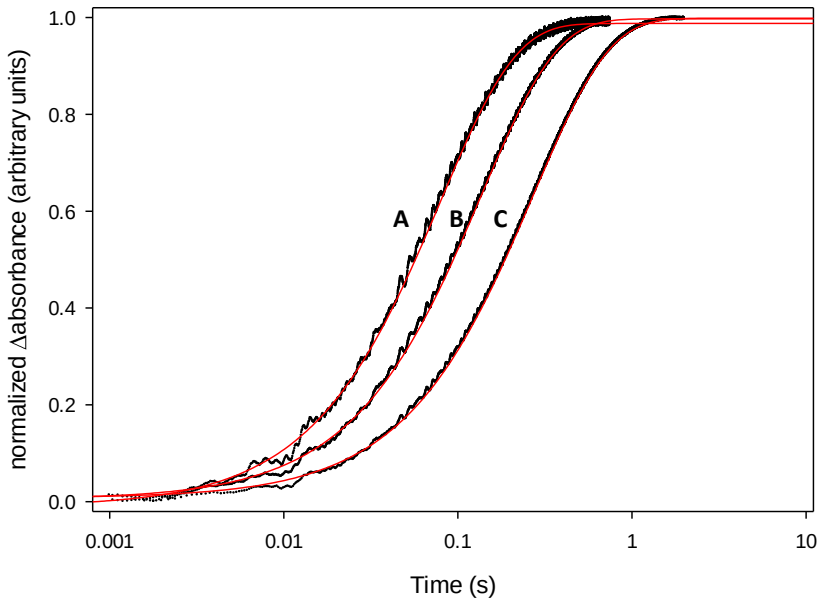

Figure 3-7: Stopped-flow traces reported as normalized changes in absorbance monitored at 324 nm as a function of time due to reaction of 20 µM NACA with 500 µM DTDP. The measured change in absorbance was normalized to the maximum difference in absorbance values (black dots). The three traces represent reactions performed at different buffer pH conditions. The reactions were performed under pseudo-first-order conditions at 12.5 °C buffered using 100 mM TRIS, 0.5 mM EDTA. The traces represent: A = pH 9.0, B = pH 8.5, C = pH 8.0. The red lines represent the best fit to a mono-exponential rise to maximum, as given by equation (3-2).

Table 3-2: Parameters associated with the best fit of equation (3-2) to stopped-flow traces obtained from the reaction of 10-150 µM NACA with DTDP. The reactions were performed under pseudo-first-order conditions ([DTDP] >> [NACA]) at 12.5 °C and the change in absorbance was monitored at 324 nm as a function of time. Each section represents a set of reactions performed under a different buffer pH condition. 100 mM Na_2HPO_4, 0.5 mM EDTA, pH 7.0; 100 mM Na_2HPO_4, 0.5 mM EDTA, pH 7.5; 100 mM TRIS, 0.5 mM EDTA, pH 8.0; 100 mM TRIS, 0.5 mM EDTA, pH 8.5; 100 mM Bis-TRIS-propane, 0.5 mM EDTA, pH 9.0; 100 mM Na_2CO_3, 0.5 mM EDTA, pH 9.5; 100 mM Na_2CO_3, 0.5 mM EDTA, pH 10.0.

pH 7.0

DTDP concentration (mM)	y_0	a	k_{app}	R^2
0.20	-0.0083 ± 0.000004	0.0561 ± 0.000004	0.2536 ± 0.00004	1.0000
0.50	0.0005 ± 0.000006	0.0571 ± 0.000005	0.6245 ± 0.0001	0.9999
1.00	0.0014 ± 0.000005	0.057 ± 0.000005	1.2483 ± 0.0002	1.0000
2.00	-0.0003 ± 0.000005	0.0566 ± 0.000005	2.5041 ± 0.0004	0.9999
3.00	0.0046 ± 0.000006	0.0565 ± 0.000006	3.647 ± 0.0008	0.9999
4.09	-0.0019 ± 0.000006	0.0568 ± 0.000005	4.6949 ± 0.0008	0.9999

pH 7.5

DTDP concentration (mM)	y_0	a	k_{app}	R^2
0.20	-0.006 ± 0.000004	0.0573 ± 0.000004	0.5876 ± 0.00008	1.0000
0.50	0.0012 ± 0.000007	0.057 ± 0.000006	1.48 ± 0.0003	0.9999
1.00	-0.0015 ± 0.000007	0.0576 ± 0.000007	2.8952 ± 0.0007	0.9999
2.00	-0.0127 ± 0.00001	0.057 ± 0.000009	5.766 ± 0.002	0.9998
3.00	-0.0054 ± 0.000008	0.0561 ± 0.000008	8.288 ± 0.002	0.9999
4.51	-0.0022 ± 0.000009	0.0564 ± 0.000008	12.193 ± 0.003	0.9999

pH 8.0

DTDP concentration (mM)	y_0	a	k_{app}	R^2
0.20	-0.0067 ± 0.000005	0.0481 ± 0.000005	1.4727 ± 0.0003	0.9999
0.50	0.000034916 ± 0.000006	0.0486 ± 0.000006	3.6781 ± 0.0008	0.9999
1.00	-0.0007 ± 0.000008	0.0486 ± 0.000008	7.33 ± 0.002	0.9998
2.00	-0.0016 ± 0.00001	0.0496 ± 0.00001	14.581 ± 0.005	0.9997
2.75	-0.0031 ± 0.00001	0.0486 ± 0.00001	19.908 ± 0.009	0.9997
3.53	0.0006 ± 0.00001	0.0489 ± 0.00001	24.85 ± 0.01	0.9996

pH 8.5

DTDP concentration (mM)	y_0	a	k_{app}	R^2
0.20	0.009 ± 0.000007	0.0465 ± 0.000006	2.8157 ± 0.0008	0.9999
0.50	-0.0031 ± 0.00001	0.0446 ± 0.00001	7.342 ± 0.003	0.9996
0.75	-0.1516 ± 0.00001	0.0416 ± 0.00001	13.013 ± 0.006	0.9996
1.00	0.0417 ± 0.00001	0.045 ± 0.00001	14.881 ± 0.007	0.9995
2.00	0.1254 ± 0.00002	0.047 ± 0.00002	29.4 ± 0.02	0.9993
3.16	-0.0053 ± 0.00002	0.0464 ± 0.00001	45.76 ± 0.03	0.9994
4.60	0.0242 ± 0.00002	0.041 ± 0.00002	62.2 ± 0.05	0.9987

pH 9.0

DTDP concentration (mM)	y_0	a	k_{app}	R^2
0.20	-0.007 ± 0.000007	0.0217 ± 0.000007	5.038 ± 0.003	0.9993
0.50	-0.0035 ± 0.00001	0.0219 ± 0.00001	12.587 ± 0.009	0.9988
1.00	0.0038 ± 0.00001	0.0218 ± 0.000009	25.97 ± 0.02	0.9987
2.00	0.0021 ± 0.00001	0.0225 ± 0.00001	47.79 ± 0.05	0.9979
2.60	-0.0019 ± 0.000006	0.0568 ± 0.000005	59.27 ± 0.07	0.9999

pH 9.5

DTDP concentration (mM)	y_0	a	k_{app}	R^2
0.20	0.0033 ± 0.000008	0.0065 ± 0.000008	6.56 ± 0.01	0.9916
1.00	0.0012 ± 0.00001	0.0137 ± 0.00001	33.36 ± 0.04	0.9960
1.94	0.0188 ± 0.00002	0.0154 ± 0.00002	57.2 ± 0.1	0.9935
2.98	0.0107 ± 0.00002	0.014 ± 0.00002	107.8 ± 0.2	0.9895

pH 10.0

DTDP concentration (mM)	y_0	a	k_{app}	R^2
0.96	0.0076 ± 0.00001	0.033 ± 0.00001	37.61 ± 0.03	0.9993
1.18	0.0061 ± 0.00001	0.0331 ± 0.00001	47.63 ± 0.03	0.9992
1.41	0.0103 ± 0.00001	0.0333 ± 0.00001	59.26 ± 0.04	0.9992

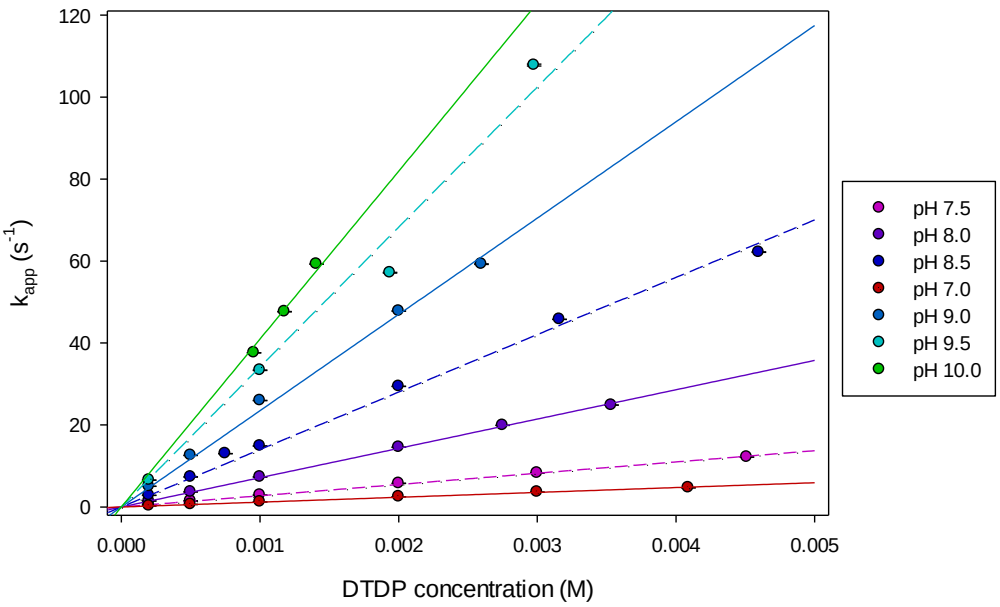

Figure 3-8: Apparent rate constant for the reaction of NACA with DTDP as a function of DTDP concentration, at various pH values. The data points correspond to the values in Table 3-2. The error bars (standard error of the exponential fits) are smaller than the data point sizes. Each colour represents different buffer pH conditions: red = 100 mM Na_2HPO_4, 0.5 mM EDTA, pH 7.0; dashed pink = 100 mM Na_2HPO_4, 0.5 mM EDTA, pH 7.5; violet = 100 mM TRIS, 0.5 mM EDTA, pH 8.0; dashed navy blue = 100 mM TRIS, 0.5 mM EDTA, pH 8.5; blue = 100 mM Bis-TRIS-propane, 0.5 mM EDTA, pH 9.0; dashed cyan = 100 mM Na_2CO_3, 0.5 mM EDTA, pH 9.5; green = 100 mM Na_2CO_3, 0.5 mM EDTA, pH 10.0. The lines are linear regression of the data points for each pH.

Table 3-3: Buffer pH, calculated [H_3O^+], and parameters of linear regression of the data in Figure 3-8. Since buffer pH was measured at room temperature, the pH at 12.5 °C (reaction temperature) was calculated using ΔpK_a/°C values for each buffer[103,104].

Room temperature pH	Temperature-corrected [H_3O^+] (M)	a (slope)	R^2
7.0	9.4E-08	1190 ± 20	0.9965
7.5	1.7E-08	2750 ± 30	0.9985
8.0	5.4E-09	7150 ± 50	0.9992
8.5	1.7E-09	14000 ± 300	0.9944
9.0	5.4E-10	23500 ± 500	0.995
9.5	2.2E-10	34000 ± 2000	0.9786
10.0	8.2E-11	41000 ± 800	0.9776

3.6. REACTION KINETICS OF OTU1ΔUBXΔZN WITH DTDP

As Otu1ΔUBXΔZN contains a single thiol group in its active-site cysteine, its reaction with DTDP can be monitored by absorbance at 324 nm similarly to NACA. However, it was also

observed that the intrinsic fluorescence of Otu1ΔUBXΔZN is quenched upon reaction with DTDP (Figure 3-9). Because fluorescence spectroscopy is more sensitive than absorbance, it permits the use of much lower enzyme concentrations. Therefore, the kinetics of the reaction of Otu1ΔUBXΔZN with DTDP were followed by monitoring the decrease in fluorescence intensity through a 320 nm longpass filter using 280 nm light as an excitation source. Between buffer pH values of 7.0 to 9.0, the apparent rates of the reactions followed by fluorescence were similar to those followed by absorbance @ 324nm within error. The time course of the reaction of Otu1ΔUBXΔZN with DTDP often follows a single exponential decay, as described by equation (3-3). (Red lines in Figure 3-9, Figure 3-10, and Figure 3-11)

$$F = y_0 + a(e^{-k_{app}t}) \qquad (3\text{-}3)$$

Where "F" is equal to the fluorescence at time "t", "y_0" is equal to the fluorescence after infinite time, and "a" is equal to the magnitude of the total change in fluorescence. However, in some cases, the progress curve is best fit to a double exponential decay, as described by equation (3-4). (Blue lines in Figure 3-9, Figure 3-10 and Figure 3-11)

$$F = y_0 + a\left(e^{-k_{app1}t}\right) + c\left(e^{-k_{app2}t}\right) \qquad (3\text{-}4)$$

Where "k_{app1}" and "k_{app2}" are two different apparent rate constants contributing to the fluorescence decay, and "a" and "c" are equal to the magnitudes of the fluorescence change associated with k_{app1} and k_{app2} respectively. An example of a reaction of Otu1ΔUBXΔZN with DTDP that displays the double-exponential phenomenon is presented in Figure 3-10, along with a visual comparison of the best fit to equation (3-3) to the best fit to equation (3-4). When present, this second, faster exponential (k_{app2}) is always associated with a small amplitude, and

was therefore considered to be a minor component. The same phenomenon is observed when the reaction is followed by absorbance at 324 nm, instead of fluorescence.

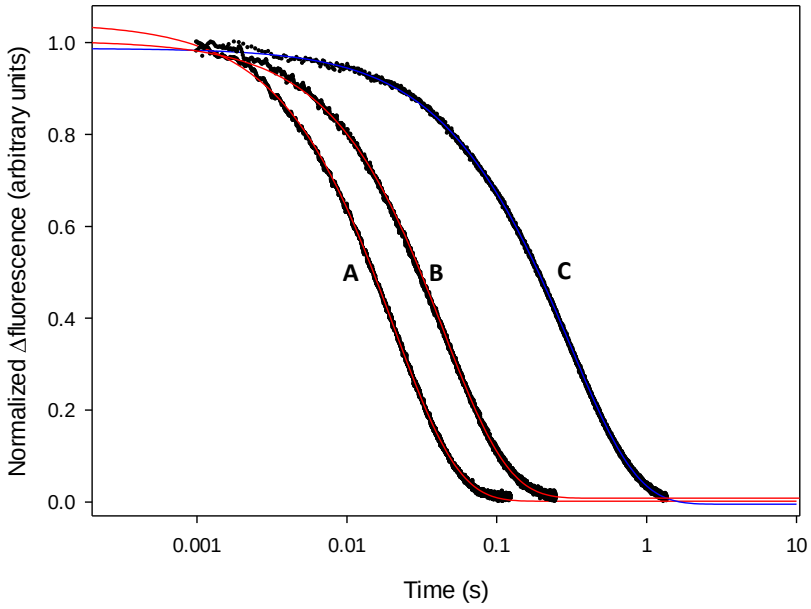

Figure 3-9: Stopped-flow traces reported as normalized changes in fluorescence intensity as a function of time due to reaction of 2 µM Otu1ΔUBXΔZN with DTDP. The reactions were monitored using excitation at 280 nm and the change in fluorescence emission intensity (measured through a 320 nm longpass filter) was normalized to the maximum difference in fluorescence values (black dots). The different traces represent different DTDP concentration values. The reactions were performed under pseudo-first-order conditions at 12.5 °C buffered using 100 mM TRIS, 0.5 mM EDTA, at pH 9.0. The traces represent: A = 2000 µM DTDP, B = 750 µM DTDP, C = 100 µM DTDP. The red lines represent the best fit to a mono-exponential decay, as given by equation (3-3). The blue line represents the best fit to a bi-exponential decay, as given by equation (3-4).

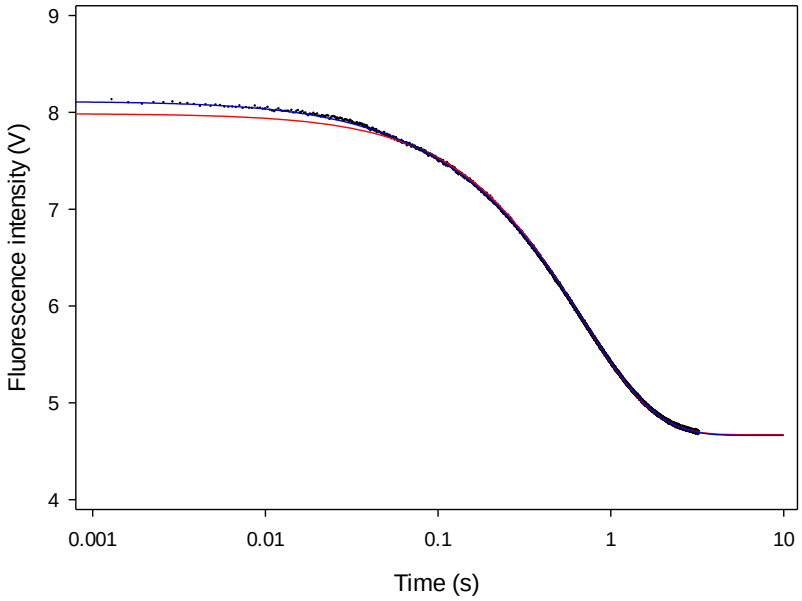

Figure 3-10: Stopped-flow trace monitoring the reaction of 2 µM Otu1ΔUBXΔZN with 100 µM DTDP reported as fluorescence intensity as a function of time. The reactions were monitored using excitation at 280 nm and the change in fluorescence emission intensity was measured through a 320 nm longpass filter (black dots). The reaction was performed under pseudo-first-order conditions at 12.5 °C buffered using 100 mM TRIS, 0.5 mM EDTA, at pH 8.5. The red line represents the best fit to a mono-exponential decay, as given by equation (3-3). The blue line represents the best fit to a bi-exponential decay, as given by equation (3-4).

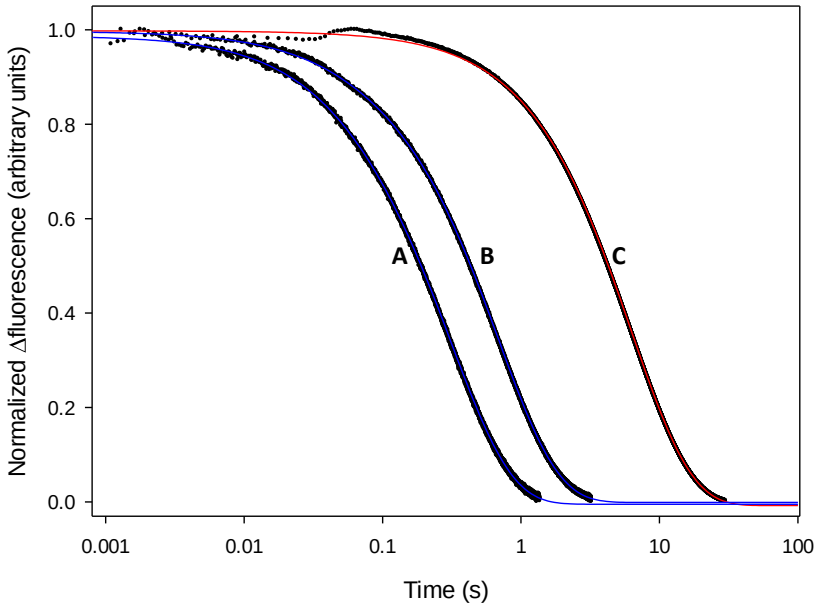

Figure 3-11: Stopped-flow traces reported as normalized changes in fluorescence intensity as a function of time due to reaction of 2 µM Otu1ΔUBXΔZN with 100uM DTDP. The reactions were monitored using excitation at 280 nm and the change in fluorescence emission intensity (measured through a 320 nm longpass filter) was normalized to the maximum difference in fluorescence values (black dots). The different traces represent reactions performed at different buffer pH conditions. The reactions were performed under pseudo-first-order conditions at 12.5 °C. The traces represent: A = 100 mM TRIS, 0.5 mM EDTA, pH 9.0; B = 100 mM TRIS, 0.5 mM EDTA, pH 8.5; C = 100 mM Na_2HPO_4, 0.5 mM EDTA pH 7.5. The red line represents the best fit to a mono-exponential decay, as given by Equation (3-3). The blue lines represent the best fit to a bi-exponential decay, as given by Equation (3-4).

Figure 3-9 depicts typical progress curves of the reaction of Otu1ΔUBXΔZN with three different concentrations of DTDP. The data reveal a possible dependence of the reaction rate on the concentration of DTDP. Figure 3-11 depicts the reaction of Otu1ΔUBXΔZN with a single DTDP concentration under different buffer pH conditions and it can be observed that the reaction rate may also depend on the pH of the solution. To investigate these trends, progress curves of the reaction of Otu1ΔUBXΔZN with a range of DTDP concentrations were collected under several different buffer pH conditions. Each reaction progress curve was fit to equation (3-3), or if necessary, equation (3-4). The fitting results are tabulated in Table 3-4. Our data do not reveal any DTDP concentration dependence or pH dependence of k_{app2}. In Figure 3-12, the apparent

rate constant of the major component (k_{app} or k_{app1}) is plotted as a function of DTDP concentration for each buffer pH condition. It can be seen that the initial slope of each DTDP dependence curve depends on the pH of the reaction. At lower pH conditions (pH 7.0 and 7.5), k_{app1} follows a quasilinear trend with respect to DTDP concentration. At higher pH conditions (pH 8.0, 8.5, and 9.0) a hyperbolic dependence of k_{app1} on DTDP concentration is observed. The fitting results are tabulated in Table 3-5. This is a significant difference from the linear trends observed for reactions with free cysteine (NACA). Therefore, reaction of DTDP with the active site cysteine of Otu1ΔUBXΔZN is not a simple bimolecular reaction. A more complicated kinetic scheme is required to fit the data. The hyperbolic trend indicates that a monomolecular step becomes rate limiting at higher DTDP concentrations and this may suggest the presence of conformational change.

Table 3-4: Parameters associated with the best fit of equation (3-3) or (3-4) to stopped-flow traces obtained from the reaction of 2 µM or 20 µM Otu1ΔUBXΔZN with DTDP. The reactions were performed under pseudo-first-order conditions ([DTDP] >> [enzyme]) at 12.5 °C and the decrease in fluorescence through a 320 nm longpass filter was monitored as a function of time using 280 nm excitation light. Each section of the table represents a set of reactions performed under a different buffer pH condition. 100 mM Na_2HPO_4, 0.5 mM EDTA, pH 7.0; 100 mM Na_2HPO_4, 0.5 mM EDTA, pH 7.5; 100 mM TRIS, 0.5 mM EDTA, pH 8.0; 100 mM TRIS, 0.5 mM EDTA, pH 8.5; 100 mM TRIS, 0.5 mM EDTA, pH 9.0; 100 mM Na_2CO_3, 0.5 mM EDTA, pH 9.5; 100 mM Na_2CO_3, 0.5 mM EDTA, pH 10.0.

pH 7.0

DTDP concentration (mM)	y_0	a	k_{app1}	c	k_{app2}	R^2
0.10	2.9947 ± 0.0002	5.4411 ± 0.0003	0.0428 ± 0.000005	-	-	1.0000
1.00	2.8266 ± 0.0002	5.3244 ± 0.0004	0.3925 ± 0.00006	0.061 ± 0.002	11.6 ± 0.5	1.0000
2.00	2.8114 ± 0.0002	5.1248 ± 0.0005	0.7604 ± 0.0002	-	-	0.9999
3.00	2.8547 ± 0.0003	5.0139 ± 0.0005	1.1059 ± 0.0003	-	-	0.9999
3.70	2.8885 ± 0.0003	4.93 ± 0.001	1.355 ± 0.0005	0.073 ± 0.003	24 ± 2	0.9999

pH 7.5

DTDP concentration (mM)	y_0	a	k_{app1}	c	k_{app2}	R^2
0.10	3.5897 ± 0.0001	4.2105 ± 0.0002	0.1596 ± 0.00002	-	-	1.0000
1.00	3.3843 ± 0.0001	4.2814 ± 0.0004	1.5982 ± 0.0003	-	-	0.9999
2.00	3.2383 ± 0.0003	4.34 ± 0.002	3.332 ± 0.002	0.384 ± 0.002	26.6 ± 0.3	0.9999
3.00	3.057 ± 0.0004	4.494 ± 0.003	5.115 ± 0.004	0.256 ± 0.003	30 ± 0.7	0.9998
4.00	2.875 ± 0.0004	4.622 ± 0.002	7.006 ± 0.004	0.186 ± 0.004	107 ± 4	0.9997
5.00	2.768 ± 0.001	4.49 ± 0.03	8.55 ± 0.03	0.4 ± 0.03	24 ± 1	0.9996

pH 8.0

DTDP concentration (mM)	y_0	a	k_{app1}	c	k_{app2}	R^2
0.10	3.998 ± 0.0001	3.251 ± 0.0003	0.698 ± 0.0001	-	-	1.0000
1.00	3.748 ± 0.0003	3.392 ± 0.006	6.472 ± 0.007	0.4 ± 0.005	22.4 ± 0.3	1.0000
2.00	3.43 ± 0.0003	3.958 ± 0.003	13.21 ± 0.01	0.188 ± 0.003	79 ± 3	1.0000
3.00	3.149 ± 0.0005	4.466 ± 0.006	18.93 ± 0.02	0.132 ± 0.006	81 ± 5	1.0000
4.00	2.943 ± 0.0003	5.014 ± 0.001	24.097 ± 0.009	-	-	1.0000
4.92	2.942 ± 0.0004	5.472 ± 0.001	27.68 ± 0.01	-	-	1.0000

pH 8.5

DTDP concentration (mM)	y_0	a	k_{app1}	c	k_{app2}	R^2
0.10	4.664 ± 0.0002	3.2706 ± 0.0006	1.4635 ± 0.0005	0.179 ± 0.001	19.4 ± 0.3	0.9999
0.50	4.3615 ± 0.0005	3.023 ± 0.008	6.71 ± 0.01	0.607 ± 0.008	23.5 ± 0.3	0.9996
1.00	4.3398 ± 0.0003	3.8419 ± 0.0008	15.082 ± 0.006	-	-	0.9997
2.00	3.9354 ± 0.0003	4.651 ± 0.001	27.69 ± 0.01	-	-	0.9995
3.00	3.4438 ± 0.0007	5.1 ± 0.002	36.05 ± 0.02	-	-	0.9993
4.00	3.0249 ± 0.0006	5.063 ± 0.002	41.86 ± 0.03	-	-	0.9992
4.98	2.8937 ± 0.0004	5.024 ± 0.001	47.12 ± 0.02	-	-	0.9995

pH 9.0

DTDP concentration (mM)	y_0	a	k_{app1}	c	k_{app2}	R^2
0.10	5.1244 ± 0.0003	2.616 ± 0.002	3.127 ± 0.002	0.233 ± 0.002	19.9 ± 0.3	0.9998
0.20	4.7325 ± 0.0002	2.587 ± 0.004	5.528 ± 0.006	0.414 ± 0.004	21.3 ± 0.2	0.9998
0.50	4.6928 ± 0.0002	2.961 ± 0.0008	16.385 ± 0.008	-	-	0.9995
0.75	4.5927 ± 0.0003	3.0087 ± 0.0007	22.76 ± 0.01	-	-	0.9996
1.00	4.2681 ± 0.0005	3.4254 ± 0.0007	29.44 ± 0.02	-	-	0.9996
1.50	4.2816 ± 0.0004	3.961 ± 0.001	40.5 ± 0.02	-	-	0.9994
2.00	3.8067 ± 0.0003	4.037 ± 0.001	49.1 ± 0.02	-	-	0.9996
2.50	3.7985 ± 0.0005	4.514 ± 0.002	55.8 ± 0.04	-	-	0.9989

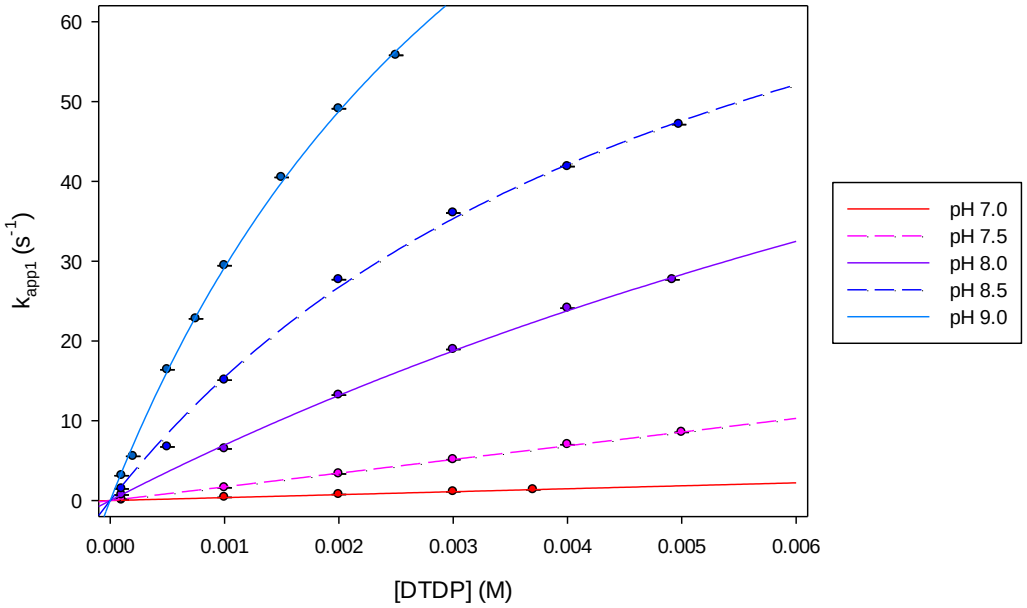

Figure 3-12: Apparent rate constant (k_{app} or k_{app1}) for the reaction of Otu1ΔUBXΔZN with DTDP as a function of DTDP concentration, at various pH values. The data points correspond to the values in Table 3-4. The error bars (standard error of the exponential fits) are smaller than the data point sizes. Each colour represents different buffer pH conditions: red = 100 mM Na_2HPO_4, 0.5 mM EDTA, pH 7.0; dashed pink = 100 mM Na_2HPO_4, 0.5 mM EDTA, pH 7.5; violet = 100 mM TRIS, 0.5 mM EDTA, pH 8.0; dashed navy blue = 100 mM TRIS, 0.5 mM EDTA, pH 8.5; blue = 100 mM TRIS, 0.5 mM EDTA, pH 9.0. The lines for pH 7.0 and 7.5 are linear regression of the data points for each pH. The curves for pH 8.0 to 9.0 represent the best fit to a hyperbola, as described in equation (4-11). Fitting results are tabulated in Table 3-5.

Table 3-5: Buffer pH, calculated [H_3O^+], and fitting parameters of the data in Figure 3-12. Since buffer pH was measured at room temperature, the pH at 12.5 °C (reaction temperature) was calculated using $\Delta pK_a/°C$ values for each buffer[103,104]. Data sets collected pH 7.0 and 7.5 were fit to a line of the form $\boldsymbol{k_{app} = a[DTDP]}$, while data sets collected at pH 8.0 to 9.0 were fit to a hyperbola described by equation (4-11).

Nominal pH	Temperature-corrected [H_3O^+] (M)	Fitting model	a	b	R^2
7.0	9.4059E-08	Linear	370 ± 3	-	0.9990
7.5	2.9744E-08	Linear	1720 ± 10	-	0.9991
8.0	5.0757E-09	Hyperbolic	120 ± 20	0.017 ± 0.003	0.9991
8.5	1.6051E-09	Hyperbolic	99 ± 8	0.0054 ± 0.0007	0.9976
9.0	5.0757E-10	Hyperbolic	148 ± 10	0.0041 ± 0.0004	0.9988

4. Discussion

The comparisons of DUB activity and thermal stability between Otu1ΔUBXΔZN and Otu1ΔUBX presented here suggest that the catalytic OTU domain of Otu1 is not affected by the presence or absence of the putative C_2H_2 zinc-binding domain. It is important to note that Ubiquitin-AMC is not the physiological substrate of Otu1 in the cell. When catalyzing cleavage of a poly-Ub chain, a second Ub molecule, rather than AMC, would be cleaved from the C-terminal glycine of the distal ubiquitin. While the role of the C_2H_2 domain is unknown, it has been suggested that it may form interactions with this proximal Ub molecule, although it is also noted that diubiquitin might be a poor substrate for Otu1ΔUBX[85]. Alternatively, the C_2H_2 domain may be involved in interacting with the cellular protein to which the polyubiquitin tag is attached. Thus, it may be possible that C_2H_2 domain removal alters deubiquitination activity of Otu1 on a more physiologically relevant substrate. This being said, the active site appears to be located far enough that minimal interactions between it and the C_2H_2 domain likely exist[85]. Therefore it is likely that the properties of the active site are similar to that of the full-length Otu1 enzyme, and all the information gained about the properties of the OTU domain alone is also applicable to this domain in the full-length Otu1 enzyme.

In order to properly determine whether the kinetics of the reaction between the probes and the active site cysteine of Otu1 reveal the presence of conformational dynamics in the enzyme active site, the kinetic details of the same reaction with a fully accessible cysteine must be acquired. Our model for a free cysteine in a peptide is NACA. It has been suggested that cysteine reacts with DTDP in a bimolecular fashion, as shown in Figure 2-1[94]. According to this scheme, the rate of the reverse reaction is negligible[94]. The rate of such a bimolecular reaction is given in equation (4-1):

$$\frac{d[4-TP]}{dt} = k_{NACA,DTDP}[NACA][DTDP] \quad (4\text{-}1)$$

Where "$\frac{d[4-TP]}{dt}$" equals the rate of 4-TP formation over time, "$k_{NACA,DTDP}$" equals the rate constant of the reaction, "[NACA]" equals the concentration of NACA, and "[DTDP]" equals the concentration of DTDP. If [DTDP] is significantly greater than [NACA], then [DTDP] remains approximately constant throughout the reaction and the reaction becomes pseudo-first order. The rate of the reaction at a given pH can then be described by equation (4-2) and (4-3):

$$\frac{d[4-TP]}{dt} = k_{obs(NACA,DTDP)}[NACA] \quad (4\text{-}2)$$

Where,

$$k_{obs(NACA,DTDP)} = k_{NACA,DTDP}[DTDP] \quad (4\text{-}3)$$

Integration of equation (4-2) gives equation (4-4):

$$[4-TP] = [NACA]_0\left(1 - e^{-k_{obs(NACA,DTDP)}t}\right) \quad (4\text{-}4)$$

Where "[4-TP]" is equal to the concentration of 4-TP at time "t", and "$[NACA]_0$" is the initial concentration of NACA. The rate constant ($k_{obs(NACA,DTDP)}$) in equation (4-4) is the same as the experimentally obtained apparent rate constant "k_{app}" in equation (3-1). Therefore, at a given pH, the apparent rate constant "k_{app}" should be a linear function of DTDP concentration, with slope equal to $k_{NACA,DTDP}$.

The linear dependence of the apparent rate constant on DTDP concentration was indeed observed, as shown in Figure 3-8. However, it was also observed that the slope of each line is dependent on the pH of the reaction. Since the ionization state of the probe does not change throughout the pH range used[94] (pH 7-10), it is likely that the mechanism of the reaction involves

deprotonation of the cysteine thiol, such that the anionic form reacts with DTDP[97]. A modified reaction scheme is presented in Figure 4-1:

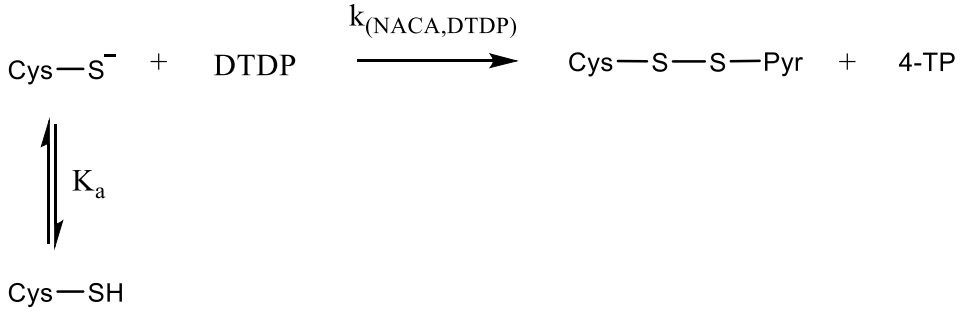

Figure 4-1: Reaction of NACA with DTDP to yield a disulfide and 4-TP.

According to this scheme, the rate of reaction is given by equation (4-5):

$$\frac{d[4-TP]}{dt} = k_{NACA,DTDP}\left(\frac{1}{1+\frac{[H_3O^+]}{K_a}}\right)[NACA][DTDP] \qquad (4\text{-}5)$$

Where "$[H_3O^+]$" is equal to the hydronium ion concentration, and "K_a" is the acid dissociation constant of the thiol group of NACA. The apparent rate constant "k_{app}" measured under pseudo-first order conditions would therefore be equal to $k_{obs(NACA,DTDP)}$ in equation (4-6):

$$k_{obs(NACA,DTDP)} = \left(\frac{1}{1+\frac{[H_3O^+]}{K_a}}\right)k_{NACA,DTDP}[DTDP] \qquad (4\text{-}6)$$

Thus, at a given pH, the apparent rate constant of the reaction is a linear function of DTDP concentration, with slope equal to $\frac{1}{1+\frac{[H_3O^+]}{K_a}}k_{NACA,DTDP}$. In Figure 4-2, the slope of each DTDP dependence line obtained from Table 3-3 is plotted as a function of $[H_3O^+]$ and fit to a rational equation of the form shown in equation (4-7):

$$slope = \frac{k_{NACA,DTDP}}{1 + \frac{1}{K_a}[H_3O^+]} \quad (4\text{-}7)$$

From the fit, the values of $k_{NACA,DTDP}$ = 45000 ± 2000 $M^{-1}s^{-1}$ and $\frac{1}{K_a}$ = 1.4 x 10^9 ± 2 x 10^8 M^{-1}, are obtained. While the pK_a of NACA has not been previously reported in the literature, our experimentally determined value of 9.15 ± 0.06 at 12.5 °C is in good agreement with reported pK_a values of N-acetylcysteine (pK_a = 9.5)[98,99] and cysteine amide (calculated pK_a = 9.1)[100] at room temperature.

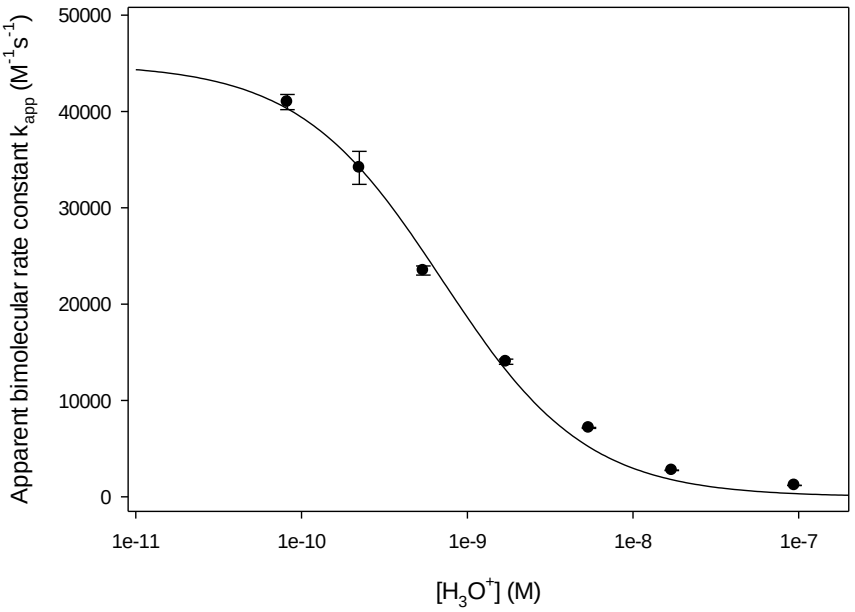

Figure 4-2: The pH dependence of the apparent bimolecular rate constant for the reaction of NACA with DTDP. The data points correspond to the values in Table 3-3. Error bars represent standard error of that value from its linear fit. The black line is the best fit to a rational function, equation (4-7), with an R^2 value of 0.993 for the fit.

4.1. MODEL ONE

If the reaction of DTDP with Otu1ΔUBXΔZN followed a bimolecular scheme as in Figure 4-1, a linear dependence of the apparent rate constant on DTDP concentration would be observed. The hyperbolic dependence that is observed instead (Figure 3-12) indicates the presence of a

monomolecular step that becomes rate-limiting at high DTDP concentrations. The simplest model to explain this phenomenon is one in which Otu1ΔUBXΔZN must undergo a conformational change prior to reaction with DTDP (Figure 4-3).

Figure 4-3: Simple scheme describing the reaction of an enzyme "E" with DTDP, yielding a disulfide and 4-TP, and involving a conformational change. (Model one)

In this model, the enzyme exists in two conformations in solution, E_{open} and E_{closed}, and only one form (E_{open}) is capable reacting with DTDP. One way to imagine this is that the active-site cysteine must be exposed to solvent in order to react with DTDP. The active-site cysteine (Cys120) appears quite buried in the crystal structure of Otu1ΔUBX solved by Messick *et al.*[85] and the CD spectrum of Otu1ΔUBXΔZN indicates that it is fully folded in solution. Therefore, it is highly unlikely that a large proportion of the population of Otu1ΔUBXΔZN enzymes exists in a conformation containing an active site cysteine that is solvent exposed. Thus, one can assume that the concentration of E_{open} in this scheme is small and the steady-state approximation applies. The rate of formation of 4-TP product is equal to the rate of consumption of unreacted enzyme. This results in a reaction rate shown in equation (4-8):

$$\frac{d[4-TP]}{dt} = -\frac{d[E_{total}]}{dt} = \frac{k_{open}[E_{total}][DTDP]}{\left(\frac{k_{open}+k_{closed}}{k_{chem}}\right)+[DTDP]} \qquad (4\text{-}8)$$

Where "$[E_{total}]$" is equal to the total concentration of unreacted Otu1ΔUBXΔZN in any conformation, and "k_{open}", "k_{closed}", and "k_{chem}", are rate constants for the reactions shown in Figure 4-3. However, a pH dependence is also observed. One possible model to account for this is presented in Figure 4-4, in which the active site cysteine may become protonated in either

enzyme conformation, preventing reaction with DTDP. Because the initial slopes of the DTDP concentration dependence curves display pH dependence (Figure 3-12), the simplest model must at least include K_{a2}, somewhat analogous to the effect of a competitive inhibitor. In reality, given the fact that in the closed conformation, the histidine residue of the catalytic triad (His222) is in close proximity to the active site cysteine[85], the value of K_{a1} is likely to be significantly larger than the value of K_{a2}. Therefore at the pH range studied, the likelihood of a protonated cysteine in the closed conformation remains small. This reduces the model to Figure 4-5.

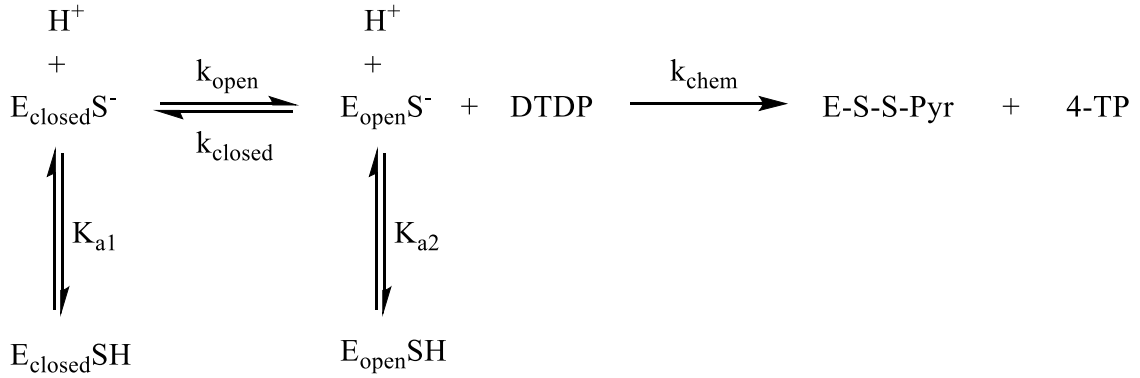

Figure 4-4: Scheme describing the reaction of an enzyme "E" with DTDP, yielding a disulfide and 4-TP, and involving both a conformational change and pH dependence. (Model one)

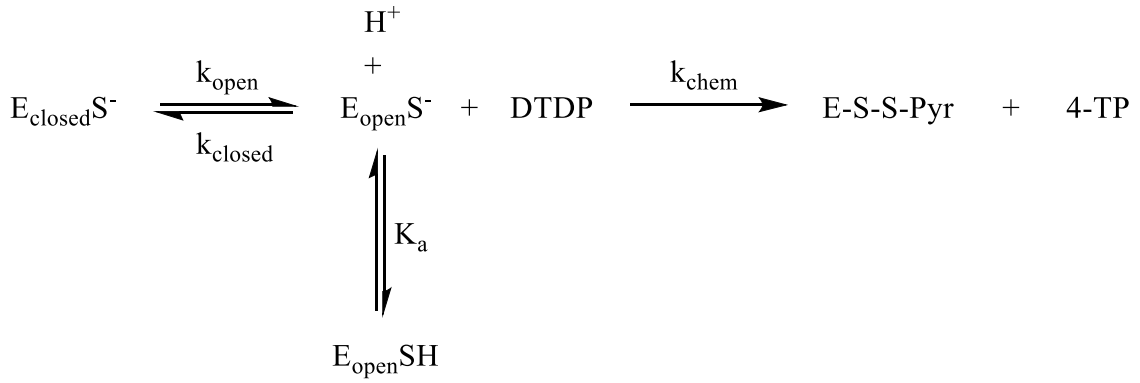

Figure 4-5: Simplified scheme describing the reaction of an enzyme "E" with DTDP, yielding a disulfide and 4-TP, and involving both a conformational change and pH dependence. (Model one)

In this model, the active site cysteine may become protonated when exposed to solvent, preventing reaction with DTDP. In solving this model, we assume that the open conformation exists in steady state and that the protonation step is extremely rapid. This results in a reaction rate shown in equation (4-9):

$$\frac{d[E_{total}]}{dt} = -\frac{k_{open}[E_{total}][DTDP]}{\left(\frac{k_{open}\left(1+\frac{[H_3O^+]}{K_a}\right)+k_{closed}}{k_{chem}}\right)+[DTDP]} \quad (4\text{-}9)$$

Where "K_a" is equal to the acid dissociation constant of the active site cysteine in the exposed conformation and "$[H_3O^+]$" is equal to the hydronium ion concentration. Since reaction with DTDP quenches intrinsic fluorescence of Otu1ΔUBXΔZN, the fluorescence intensity is proportional to the total amount of unreacted enzyme, and reaction time course can be monitored by following the decrease in fluorescence intensity over time. Integration of equation (4-9) results in a mono-exponential decay with an apparent rate constant "k_{app}" equal to $k_{obs(\text{Otu1ΔUBXΔZN,DTDP})}$ described in equation (4-10):

$$k_{obs(\text{Otu1ΔUBXΔZN,DTDP})} = \frac{k_{open}[DTDP]}{\left(\frac{k_{open}\left(1+\frac{[H_3O^+]}{K_a}\right)+k_{closed}}{k_{chem}}\right)+[DTDP]} \quad (4\text{-}10)$$

The fast, minor component (k_{app2}) observed in the fluorescence traces (e.g. Figure 3-10) may arise from the approach of the system towards steady state at the beginning of the reaction. This model predicts that the major decay component (k_{app} or k_{app1}) should follow a hyperbolic dependence on DTDP concentration, as shown in equation (4-11):

$$k_{app} = \frac{a[DTDP]}{b+[DTDP]} \quad (4\text{-}11)$$

Where “b” is pH dependent, and “a” is a pH-independent parameter. If the data at each pH in Figure 3-12 are correlated with equation (4-11), it can be observed that the value of “a” is minimally affected by pH, while “b” shows significant pH dependence (Table 3-5). In Figure 4-6, the data of Figure 3-12 are plotted and each set is fit to equation (4-11) with a globally shared “a” value.

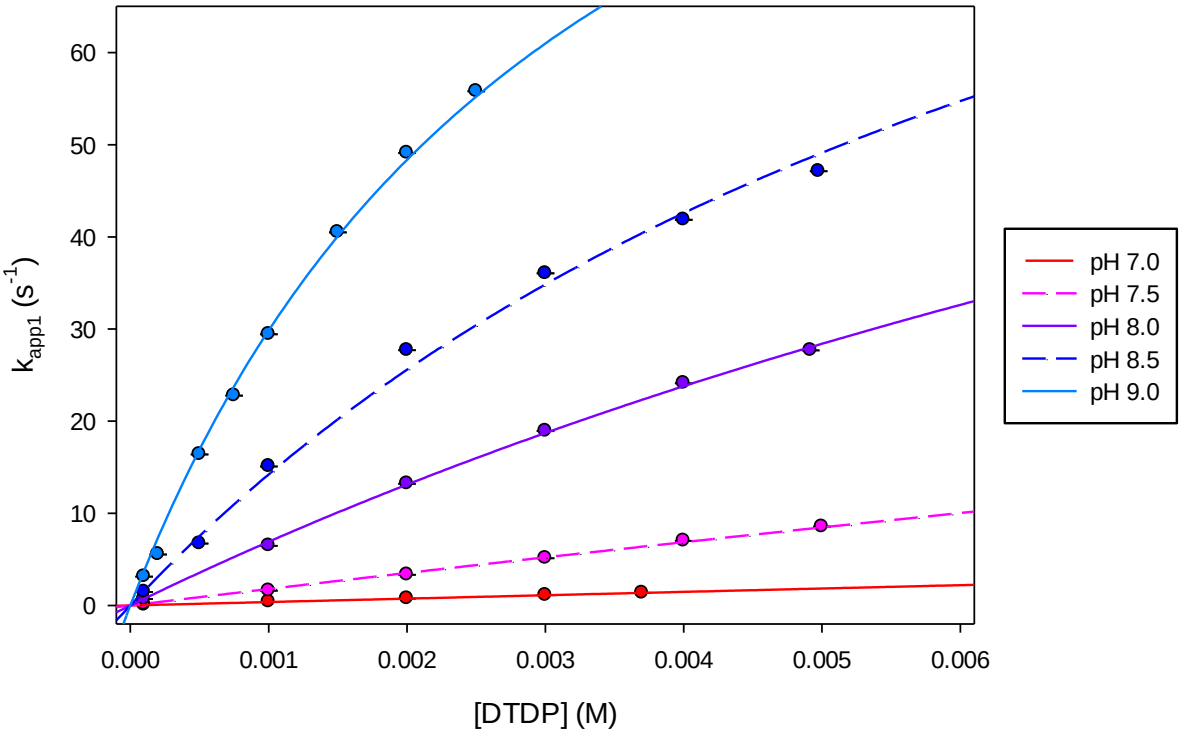

Figure 4-6: Apparent rate constant (k_{app} or k_{app1}) for the reaction of Otu1ΔUBXΔZN with DTDP as a function of DTDP concentration, at various pH values. The data points correspond to the values in Table 3-4. The error bars (standard error of the exponential fits) are smaller than the data point sizes. Each colour represents different buffer pH conditions: red = 100 mM Na_2HPO_4, 0.5 mM EDTA, pH 7.0; dashed pink = 100 mM Na_2HPO_4, 0.5 mM EDTA, pH 7.5; violet = 100 mM TRIS, 0.5 mM EDTA, pH 8.0; dashed navy blue = 100 mM TRIS, 0.5 mM EDTA, pH 8.5; blue = 100 mM TRIS, 0.5 mM EDTA, pH 9.0. The lines represent the best fit to equation (4-11) with a globally shared “a” parameter. The fitting results are tabulated in Table 4-1.

Table 4-1: Buffer pH, calculated [H_3O^+], and fitting parameters of the data in Figure 4-6. "a" and "b" are parameters for the best fit to equation (4-11) with a globally shared "a" parameter. Since buffer pH was measured at room temperature, the pH at 12.5 °C (reaction temperature) was calculated using ΔpK_a/°C values for each buffer[103,104].

Nominal pH	Temperature-corrected [H_3O^+] (M)	a	b	R^2
7.0	9.4E-08	127 ± 7	0.3 ± 0.1	0.999
7.5	3.0E-08	127 ± 7	0.070 ± 0.006	0.998
8.0	5.1E-09	127 ± 7	0.017 ± 0.001	0.999
8.5	1.6E-09	127 ± 7	0.0080 ± 0.0006	0.994
9.0	5.1E-10	127 ± 7	0.0033 ± 0.0003	0.998

According to equations (4-10) and (4-11), the "a" parameter is equal to k_{open}. Therefore, by this model, we determine k_{open} = 127 ± 7 s^{-1}. Also according to these equations, the "b" value is linearly dependent on [H_3O^+]. This is made clearer when rearranged in equation (4-12):

$$b = \left(\frac{k_{open}}{k_{chem}K_a}\right)[H_3O^+] + \left(\frac{k_{open} + k_{closed}}{k_{chem}}\right) \quad (4\text{-}12)$$

To investigate this dependence, the "b" parameter values obtained from the global fit in Figure 4-6 and Table 4-1 were plotted as a function of [H_3O^+], as shown in Figure 4-7. The best fit to a line of the form in equation (4-12) is also shown. The data point obtained at pH 7.0 was excluded due to its large error. From the fit, the values of $\frac{k_{open}}{k_{chem}K_a}$ = 2.23 x 10^6 ± 8 x 10^4 (unitless) and $\frac{k_{open}+k_{closed}}{k_{chem}}$ = 0.004 ± 0.001 M are obtained. Assuming that the rate constant of the reaction of DTDP with the exposed, anionic cysteine of Otu1ΔUBXΔZN (k_{chem}) is no greater than the rate constant of its reaction with NACA ($k_{NACA,DTDP}$ = 45000 ± 2000 $M^{-1}s^{-1}$), then k_{closed} will not be greater than 53 ± 50 s^{-1}.

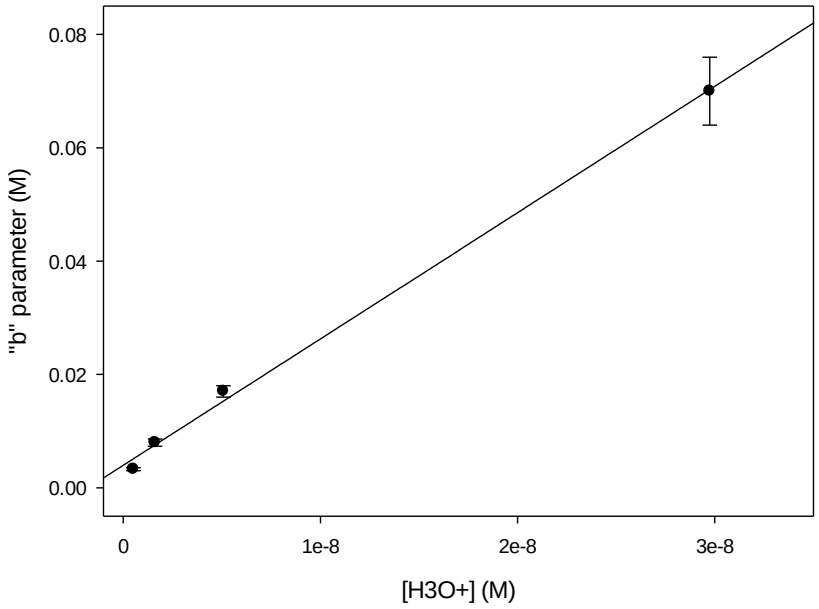

Figure 4-7: The pH dependence of the apparent rate constant for the reaction of Otu1ΔUBXΔZN with DTDP. The data points correspond to the "b" parameter and $[H_3O^+]$ values in Table 4-1. Error bars represent standard error of that value from its linear fit. Black line is the best fit to equation (4-12), with an R^2 value of 0.998 for the fit.

In order for the steady-state approximation to be valid, the sum of k_{closed} and k_{chem}[DTDP] must be significantly greater than k_{open}, such that the concentration of $E_{open}S^-$ is low and nearly constant during the reaction. The range of DTDP concentrations used in this study gives an average k_{chem}[DTDP] of around 100. This plus the values of k_{closed} (53 ± 50 s^{-1}) and k_{open} (127 ± 7 s^{-1}) calculated using the model in Figure 4-5 does not satisfy the requirement for steady state. Therefore, this model does not adequately describe the data presented here.

4.2. MODEL TWO

An alternative model is presented in Figure 4-8. In this scheme, DTDP must first bind to the Otu1ΔUBXΔZN enzyme, and then the conformational change necessary for reaction may occur.

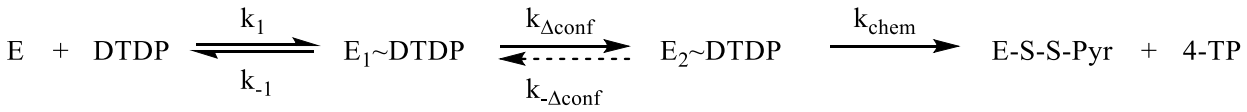

Figure 4-8: Simple scheme describing the reaction of an enzyme "E" with DTDP, yielding a disulfide and 4-TP, and involving complex formation prior to a conformational change. (Model two).

In solving this scheme for the rate of consumption of total unreacted enzyme, we assume that since the local concentration of DTDP is high in E_2~DTDP complex, the rate of the chemical step (k_{chem}) is significantly greater than the conformational change ($k_{\Delta conf}$) so that [E_2~DTDP] is at steady state. We also assume that complex formation between DTDP and the enzyme is rapid. This results in the following equation:

$$\frac{d[E_{total}]}{dt} = -\frac{\frac{k_{\Delta conf}k_{chem}}{k_{\Delta conf}+k_{chem}+k_{-\Delta conf}}[E_{total}][DTDP]}{\left(\frac{k_{-1}}{k_1}\right)\left(\frac{k_{chem}+k_{-\Delta conf}}{k_{chem}+k_{-\Delta conf}+k_{\Delta conf}}\right)+[DTDP]} \qquad (4\text{-}13)$$

Since the ΔG of unfolding for most proteins is small, the ΔG of the conformational change is likely also small. If so, the magnitude of the activation energy barriers for the forward and reverse conformational changes are likely similar, and thus so are the associated rate constants. If we assume that the rate of the chemical step (k_{chem}) is fast compared to both the forward and reverse rates of the conformational change ($k_{\Delta conf}$ and $k_{-\Delta conf}$), the model can be reduced to the scheme presented in Figure 4-9, in which k_2 is approximately equal to $k_{\Delta conf}$. This also results in reducing equation (4-13) to equation (4-14).

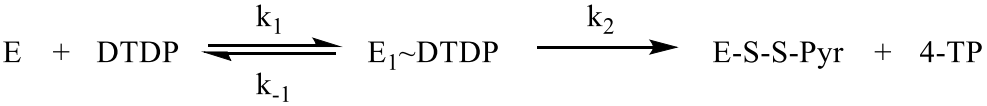

Figure 4-9: Reduced scheme describing the reaction of an enzyme "E" with DTDP, yielding a disulfide and 4-TP, and involving complex formation prior to a conformational change. (Model two).

$$\frac{d[E_{total}]}{dt} = -\frac{k_2[E_{total}][DTDP]}{\left(\frac{k_{-1}}{k_1}\right) + [DTDP]} \quad (4\text{-}14)$$

Integration of equation (4-14) results in a mono-exponential decay with an apparent rate constant "k_{app}" equal to $k_{obs(\mathrm{Otu1\Delta UBX\Delta ZN,DTDP})}$ described in equation (4-15):

$$k_{obs(\mathrm{Otu1\Delta UBX\Delta ZN,DTDP})} = \frac{k_2[DTDP]}{\left(\frac{k_{-1}}{k_1}\right) + [DTDP]} \quad (4\text{-}15)$$

As with the previous model, this model predicts that the observed rate constant should follow a hyperbolic dependence on DTDP concentration. As can be seen in Figure 3-12, the rate constant associated with the major component (k_{app} or k_{app1}) does indeed follow a hyperbolic dependence on DTDP concentration at higher pH values. The fast, minor component (k_{app2}) also observed in the fluorescence traces (e.g. Figure 3-10) may arise from the establishment of the binding equilibrium at the beginning of the reaction.

The trends observed in the DTDP concentration dependence of the apparent rate constant (k_{app}) in Figure 3-12 reveal that the initial slope depends on the pH of the solution. This indicates that the simplest model must include a rapid acid-base equilibrium in the first step. In other words, protonation prevents binding of DTDP to the enzyme, analogous to the effect of a competitive inhibitor in Michaelis-Menten kinetics. This modification is represented in Figure 4-10.

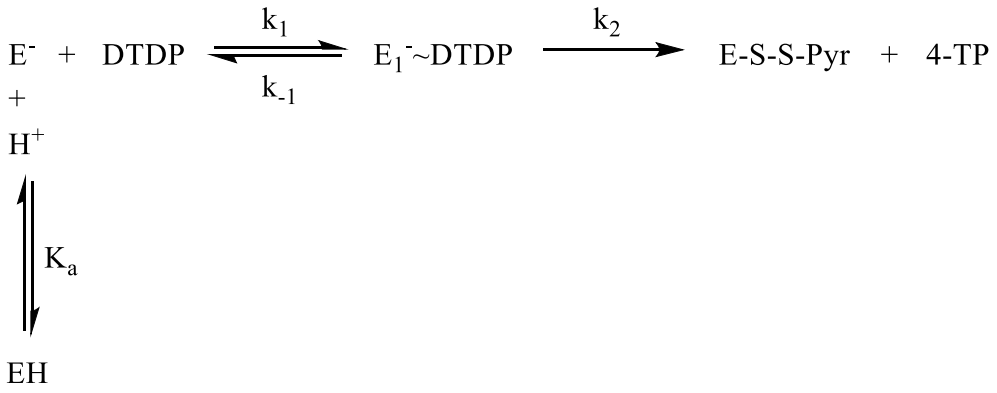

Figure 4-10: Reduced scheme describing the reaction of an enzyme "E" with DTDP, modified to account for pH dependence. (Model two).

Solving the scheme in Figure 4-10 for the rate of consumption of total unreacted enzyme and integration of that solution results in a mono-exponential decay with an apparent rate constant "k_{app}" equal to $k_{obs(\mathrm{Otu1\Delta UBX\Delta ZN,DTDP})}$ described in equation (4-16):

$$k_{obs(\mathrm{Otu1\Delta UBX\Delta ZN,DTDP})} = \frac{k_2[DTDP]}{\left(1 + \frac{[H_3O^+]}{K_a}\right)\left(\frac{k_{-1}}{k_1}\right) + [DTDP]} \qquad (4\text{-}16)$$

Again, this model predicts that the observed rate constant should follow a hyperbolic dependence on DTDP concentration, in a form similar to equation (4-11). However, the microscopic rate constants in this equation clearly differ from equation (4-10). Thus, the "a" parameter value of 127 ± 7 s^{-1} obtained from the global fit in Figure 4-6 and Table 4-1 represents k_2, which is approximately equal to $k_{\Delta conf}$ in the model presented in Figure 4-10.

According to equation (4-16), the initial slope of the DTDP dependence curves (Figure 4-6) follows a rational dependence on $[H_3O^+]$ as shown in equation (4-17):

$$Initial\ slope = \frac{\frac{k_2 k_1}{k_{-1}}}{1 + \frac{1}{K_a}[H_3O^+]} \qquad (4\text{-}17)$$

In Figure 4-11 the initial slopes are plotted as a function of $[H_3O^+]$. From the fit, the values of $\frac{k_2 k_1}{k_{-1}}$ = 1.0 x 10^5 ± 2 x 10^4 $M^{-1}s^{-1}$ and $\frac{1}{K_a}$ = 3.0 x 10^9 ± 8 x 10^8 M^{-1} are obtained. This results in a dissociation constant $\frac{k_{-1}}{k_1}$ = 1.3 x 10^{-3} ± 3 x 10^{-4} M and pKa = 9.5 ± 0.1. This pKa is not far from the experimentally determined value for NACA. Additional data points at higher pH values would be helpful for improving confidence in the fit in Figure 4-11, although fluorescence traces of the reaction at pH values above 9.0 were noisy and unreliable.

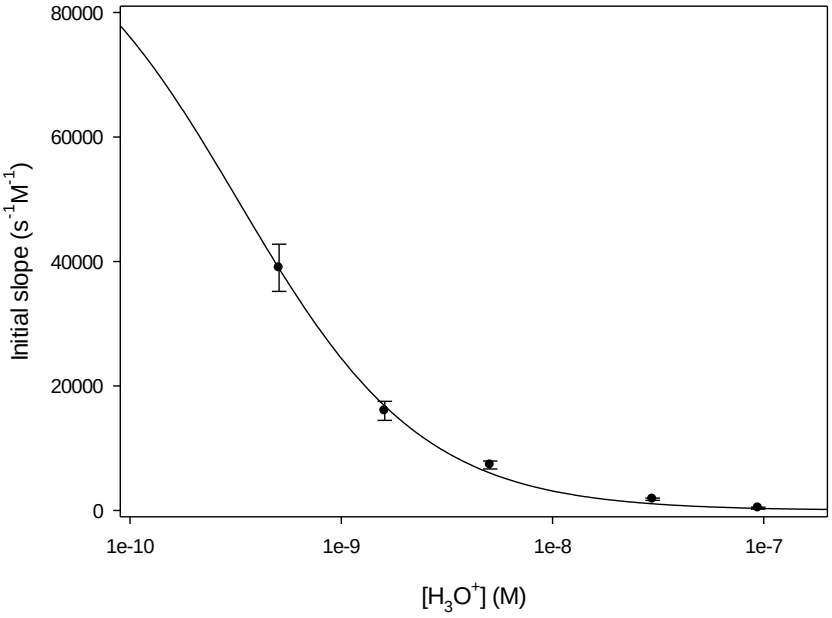

Figure 4-11: The pH dependence of the apparent rate constant for the reaction of Otu1ΔUBXΔZN with DTDP. Initial slopes obtained from fits in Table 4-1. The black line is the best fit to a rational function, equation (4-17), with an R^2 value of 0.997 for the fit.

DTDP is neutral within the pH range used in this study and relatively hydrophobic, allowing it to access cysteines in buried or hydrophobic areas of a protein[94]. In the crystal structure of Otu1 solved by Messick *et al.*[85], the catalytic cysteine residue (Cys120) is quite buried within the active-site groove. Additionally, among other interactions, Otu1 employs several hydrophobic interactions to mediate contact with the distal ubiquitin of its substrate, both near and far from

the active site, including to a hydrophobic patch of ubiquitin[85]. Accordingly, it is not surprising that DTDP would associate near hydrophobic regions of Otu1 and form a complex as an initial step in the reaction. A small dissociation constant such as the one calculated here ($K_D = \frac{k_{-1}}{k_1}$ = 1.3 x 10^{-3} ± 3 x 10^{-4} M) would be expected for such a weak interaction.

If the pH range used in this study affected the chemical reaction step as it did in NACA, we could not have been able to observe a difference due to the comparatively slow conformational change. It is interesting that the apparent rate of the conformational change was not affected by buffer pH. In our model of the reaction, protonation instead prevents DTDP from binding to Otu1ΔUBXΔZN. To explain this, it is possible that deprotonation results in the loss of a charge or hydrogen bond that is important in holding two structural components together (such as a salt bridge). Deprotonation may then allow greater flexibility in the enzyme structure and improve access to a DTDP binding site. If so, the new dynamic motion must be quite fast. This property could be a regulatory feature that functions to lock the enzyme into a more rigid or inaccessible form at physiological pH and prevents reaction with its substrate, until a conformational change into catalytic form is induced by a binding partner.

It has been demonstrated that enzyme conformational changes and dynamic motions involved in catalysis are also sampled by the free enzymes in the absence of substrate[10,33,40]. The slow conformational change observed here ($k_{\Delta conf}$) may therefore be important in the catalytic mechanism of Otu1. While the timescale of the slow conformational change has been calculated in this study (127 ± 7 s^{-1}), no information is provided about what structural components are involved in the motion.

A potential candidate is the WGGA loop of Otu1 that covers the active site when bound to substrate in the crystal structure[85]. Trp175 on this loop has been shown to form van der Waals contacts with the C-terminal residues of the distal ubiquitin, apparently to help push it towards the catalytic cysteine residue of the enzyme, and its mutation eliminates the enzyme's DUB activity[85]. It's possible that Trp175 provides a similar function during the reaction with DTDP. However, the slow timescale of the observed conformational change suggests that it involves a larger amplitude motion that includes more of the enzyme structure[24].

His222 is an important member of the catalytic triad. In the catalytic mechanism of cysteine proteases, it functions to deprotonate the cysteine residue[79]. Not unexpectedly, mutation of His222 to alanine destroys DUB activity[85]. While His222 and Cys120 are nearby in the crystal structure of Otu1ΔUBX bound to Ub substrate, they are distant in sequence and on entirely separate secondary structural elements[85]. Therefore, it is plausible that Otu1 can adopt a catalytically inactive conformation in which His222 and Cys120 are spatially distant. If so, labelling of Cys120 with DTDP could require a conformational change to bring the two residues close and deprotonate the cysteine thiol. This is not unreasonable considering the Otu1 crystal structure: the active site groove that surrounds the C-terminal tail of the distal Ub is quite compact, and includes the WGGA loop that wraps all the way around to completely envelop the tail. If a polyubiquitin chain is the physiological substrate of Otu1, it would not be able to thread through the Otu1 active site groove in this closed conformation. Some of the Otu1 catalytic OTU domain structure would need to separate and open up in order to then wrap around the Ub-Ub linker and adopt the conformation observed in the crystal structure. In opening up, Cys120 and His222 may become separated. There is precedence for this model: in the crystal structure of herpes virus-associated ubiquitin-specific protease (HAUSP), a USP-type deubiquitinase, the

cysteine and histidine residues of the catalytic triad are too far from one another for catalysis and must be brought together by substrate-induced conformational change[101]. It would be interesting to see how mutation of His222 affects the monomolecular step observed in the reaction of Otu1ΔUBXΔZN with DTDP.

5. Summary and Future Directions

In this work, we have studied the properties of the active site of the Otu1 enzyme by overexpressing and purifying the catalytic OTU domain. We have shown that its biophysical properties and catalytic activity are minimally affected by removal of the putative C_2H_2 zinc-binding domain. We have probed the OTU domain using the cysteine-labelling molecule DTDP. The labelling reaction kinetics have been followed using stopped-flow spectroscopy methods and have revealed the presence of a conformational change with a frequency of $127 \pm 7\ s^{-1}$. This conformational change may potentially play a role in the enzyme's catalytic mechanism.

To help corroborate our interpretation of the results of this study, the labelling reaction kinetics of DTDP with the unfolded state of Otu1ΔUBXΔZN could be followed in the presence of a strong denaturant, such as urea. If the rate-limiting step observed in the DTDP concentration dependence plots (Figure 3-12) indeed arises from a conformational change, reaction with unfolded enzyme should display a linear dependence on DTDP concentration.

In order to further investigate the effect of the removal of the putative C_2H_2 domain on the physiological function of Otu1, additional activity assays could be performed using a diubiquitin FRET probe pair as a substrate[102]. Cleavage of this substrate would occur between two ubiquitin molecules, and therefore would likely better represent the physiological substrate of Otu1 than Ub-AMC. If important interactions exist between the putative C_2H_2 domain and the proximal ubiquitin molecule when acting on a poly-ubiquitin chain, they may manifest as differences in the kinetics of DUB activity between Otu1ΔUBX and Otu1ΔUBXΔZN when acting on this substrate.

The most important unanswered question in this study is what aspect of the OTU structure is undergoing the observed conformational change. Now that the timescale of the dynamic motion is known, NMR spectroscopy could reveal which structural components move at this timescale at atomic resolution. Specifically, magnetization-exchange or CPMG relaxation dispersion experiments may be particularly helpful at this timescale[41].

As there is currently no structure available of Otu1 in the absence of bound substrate, it may be useful to attempt to crystallize Otu1ΔUBXΔZN alone and determine its structure using X-ray diffraction. The structure of the free OTU domain may reveal a different conformation than the substrate-bound state solved by Messick *et al*.[85], such as an open, binding-competent conformation. If crystallization proves difficult without a binding partner for the enzyme, NMR spectroscopy could allow for solving the OTU domain structure free in solution.

6. References

1. Callender R, Dyer RB. The dynamical nature of enzymatic catalysis. *Acc Chem Res*. 2015;48(2):407-413.

2. Radzicka A, Wolfenden R. A proficient enzyme. (orotidine 5'-phosphate decarboxylase). *Science*. 1995;267(5194):90.

3. Berg JM. *Biochemistry.* 5th ed.. ed. New York: New York : W.H. Freeman; 2002.

4. Thauer RK. Citric- acid cycle, 50 years on. *European Journal of Biochemistry*. 1988;176(3):497-508.

5. Endo A. The discovery and development of hmg- coa reductase inhibitors. *J Lipid Res*. 1992;33(11):1569-1582.

6. Shchemelinin I, Sefc L, Necas E. Protein kinases, their function and implication in cancer and other diseases. *Folia Biol*. 2006;52(3):81-100.

7. Wuethrich K. Protein structure determination in solution by NMR spectroscopy. *J Biol Chem*. 1990;265(36):22059-22062.

8. Dunaway-Mariano D. Enzyme function discovery. *Structure*. 2008;16(11):1599-1600.

9. Anfinsen CB. Principles that govern the folding of protein chains. *Science*. 1973;181(4096):223-230.

10. Henzler-Wildman K, Kern D. Dynamic personalities of proteins. *Nature*. 2007;450(7172):964-972.

11. Arora K(, Hammes-Schiffer S, Klinman J, SpringerLink (Online service). *Dynamics in enzyme catalysis.* Berlin: Berlin : Springer; 2013.

12. Pravda L, Berka K, Svobodová Vareková R, et al. Anatomy of enzyme channels. *BMC Bioinformatics*. 2014;15.

13. Blake CCF, Koenig DF, Mair GA, North ACT, Phillips DC, Sarma VR. Structure of hen egg- white lysozyme: A three- dimensional fourier synthesis at 2 Å resolution. *Nature*. 1965;206(4986):757.

14. Haldane J. S.(1930) enzymes. . 1930.

15. PAULING L. Molecular architecture and biological reactions. *Chem Eng News Archive*. 1946;24(10):1375-1377.

16. Cornish-Bowden A. *Fundamentals of enzyme kinetics.* 4th rev. ed.. ed. Weinheim: Weinheim : Wiley-VCH; 2012.

17. Nelson DL(L. *Lehninger principles of biochemistry.* 5th ed.. ed. New York: New York : W.H. Freeman; 2008.

18. Wolfenden R. Transition state analogues for enzyme catalysis. *Nature*. 1969;223(5207):704.

19. Singh V, Lee JE, Núñez S, Howell PL, Schramm VL. Transition state structure of 5'-methylthioadenosine/ S- adenosylhomocysteine nucleosidase from escherichia coli and its similarity to transition state analogues. *Biochemistry (N Y)*. 2005;44(35):11647.

20. Gutierrez JA, Luo M, Singh V, et al. Picomolar inhibitors as transition- state probes of 5'-methylthioadenosine nucleosidases. *ACS chemical biology*. 2007;2(11):725.

21. Singh V, Evans GB, Lenz DH, et al. Femtomolar transition state analogue inhibitors of 5'-methylthioadenosine/ S- adenosylhomocysteine nucleosidase from escherichia coli. *The Journal of biological chemistry*. 2005;280(18):18265.

22. Alexandrova AN, Röthlisberger D, Baker D, Jorgensen WL. Catalytic mechanism and performance of computationally designed enzymes for kemp elimination. *J Am Chem Soc*. 2008;130(47):15907.

23. Steven DS, Vern LS. Enzymatic transition states and dynamic motion in barrier crossing. *Nature Chemical Biology*. 2009;5(8):551.

24. Callender R, Dyer R. Advances in time- resolved approaches to characterize the dynamical nature of enzymatic catalysis. *Chem Rev*. 2006;106(8):3031-3042.

25. Schwartz SD. Protein dynamics and the enzymatic reaction coordinate. *Top Curr Chem*. 2013;337:189.

26. Kipp DR, Silva RG, Schramm VL. Mass- dependent bond vibrational dynamics influence catalysis by HIV- 1 protease. *J Am Chem Soc*. 2011;133(48):19358.

27. Wang Z, Singh P, Czekster CM, Kohen A, Schramm VL. Protein mass- modulated effects in the catalytic mechanism of dihydrofolate reductase: Beyond promoting vibrations.(report). *J Am Chem Soc*. 2014;136(23):8333-8341.

28. Rout MK, Hodge CD, Markin CJ, et al. Stochastic gate dynamics regulate the catalytic activity of ubiquitination enzymes. *J Am Chem Soc*. 2014;136(50):17446.

29. Henzler-Wildman K, Lei M, Thai V, Jordan Kerns S, Karplus M, Kern D. A hierarchy of timescales in protein dynamics is linked to enzyme catalysis. *Nature*. 2007;450.

30. Barends TRM, Foucar L, Ardevol A, et al. Direct observation of ultrafast collective motions in CO myoglobin upon ligand dissociation. *Science (New York, N.Y.)*. 2015;350(6259):445.

31. Avvakumov GV, Walker JR, Xue S, et al. Amino- terminal dimerization, NRDP1-rhodanese interaction, and inhibited catalytic domain conformation of the ubiquitin-specific protease 8 (USP8). *The Journal of biological chemistry*. 2006;281(49):38061.

32. Magnus Wolf-Watz, Thai V, Katherine Henzler-Wildman, Hadjipavlou G, Elan ZE, Kern D. Linkage between dynamics and catalysis in a thermophilic- mesophilic enzyme pair. *Nature Structural & Molecular Biology*. 2004;11(10):945.

33. Beach H, Cole R, Gill ML, Loria JP. Conservation of (mu)s- ms enzyme motions in the apo- and substrate- mimicked state. *J Am Chem Soc*. 2005;127(25):9167-9176.

34. Khajehpour M, Liu S, Zhadin N, Zhang Z, Callender R. Loop dynamics and ligand binding kinetics in the reaction catalyzed by the yersinia protein tyrosine phosphatase. *Biochemistry (Wash)*. 2007;46(14):4370-4378.

35. Bhabha G, Lee J, Ekiert DC, et al. A dynamic knockout reveals that conformational fluctuations influence the chemical step of enzyme catalysis.(REPORTS)(author abstract)(report). *Science*. 2011;332(6026):234.

36. Whittier SK, Hengge AC, Loria JP. Conformational motions regulate phosphoryl transfer in related protein tyrosine phosphatases.(REPORTS)(author abstract). *Science*. 2013;341(6148):899.

37. Sorensen JL, Stetefeld J. Kinemage of action - proposed reaction mechanism of glutamate- 1-semialdehyde aminomutase at an atomic level. *Biochem Biophys Res Commun*. 2011;413(4):572.

38. Ergel B, Gill ML, Brown L, Yu B, Palmer AG, Hunt JF. Protein dynamics control the progression and efficiency of the catalytic reaction cycle of the escherichia coli DNA-repair enzyme AlkB. *The Journal of biological chemistry*. 2014;289(43):29584.

39. Eisenmesser EZ, Bosco DA, Akke M, Kern D. Enzyme dynamics during catalysis. *Science (New York, N.Y.)*. 2002;295(5559):1520.

40. Eisenmesser EZ, Millet O, Labeikovsky W, et al. Intrinsic dynamics of an enzyme underlies catalysis. *Nature*. 2005;438(7064):117.

41. Mittermaier AK, Kay LE. Observing biological dynamics at atomic resolution using NMR. *Trends Biochem Sci*. 2009;34(12):601-611.

42. Kleckner IR, Foster MP. An introduction to NMR-based approaches for measuring protein dynamics. *BBA - Proteins and Proteomics*. 2011;1814(8):942-968.

43. Sprangers R, Hwang PM, Houry WA, Kay LE. Quantitative NMR spectroscopy of supramolecular complexes: Dynamic side pores in ClpP are important for product release. *Proc Natl Acad Sci U S A*. 2005;102(46):16678-16683.

44. Wider G, Neri D, Wüthrich K. Studies of slow conformational equilibria in macromolecules by exchange of heteronuclear longitudinal 2-spin-order in a 2D difference correlation experiment. *J Biomol NMR*. 1991;1(1):93-98.

45. Boehr DD, Mcelheny D, Dyson HJ, Wright PE. The dynamic energy landscape of dihydrofolate reductase catalysis. *Science*. 2006;313(5793):1638-1642.

46. Vallurupalli P, Hansen DF, Kay LE. Structures of invisible, excited protein states by relaxation dispersion NMR spectroscopy. *Proc Natl Acad Sci U S A*. 2008;105(33):11766.

47. Kasinath V, Fu Y, Sharp KA, Wand AJ. A sharp thermal transition of fast Aromatic-Ring dynamics in ubiquitin. *Angewandte Chemie International Edition*. 2015;54(1):102-107.

48. Lange OF, Lakomek N, Farès C, et al. Recognition dynamics up to microseconds revealed from an RDC-derived ubiquitin ensemble in solution. *Science (New York, N.Y.)*. 2008;320(5882):1471.

49. Dyer RB, Reddish MJ, Vaughn MB, Fu R. Ligand- dependent conformational dynamics of dihydrofolate reductase.(report). . 2016;55(10):1485-1493.

50. Peng H, Egawa T, Chang E, Deng H, Callender R. Mechanism of thermal adaptation in the lactate dehydrogenases.(report). . 2015;119(49):15256-15262.

51. Pandit A, Ma H, van Stokkum IHM, Gruebele M, Grondelle Rv. Time- resolved dissociation of the light- harvesting 1 complex of rhodospirillum rubrum, studied by infrared laser temperature. *Biochemistry (N Y)*. 2002;41(51):15115.

52. Khajehpour M. Personal communication. . 2016.

53. Gutman M, Huppert D, Pines E. The pH jump: A rapid modulation of pH of aqueous solutions by a laser pulse. *J Am Chem Soc*. 1981;103(13):3709-3713.

54. Viappiani C, Bonetti G, Carcelli M, Ferrari F, Sternieri A. Study of proton transfer processes in solution using the laser induced p H - jump: A new experimental setup and an improved data analysis based on genetic algorithms. *Rev Sci Instrum*. 1998;69(1):270-276.

55. Causgrove TP, Dyer RB. Nonequilibrium protein folding dynamics: Laser-induced pH-jump studies of the helix–coil transition. *Chem Phys*. 2006;323(1):2-10.

56. Bagshaw CR. Stopped-flow techniques. In: Roberts GCK, ed. *Encyclopedia of biophysics.* Berlin, Heidelberg: Springer Berlin Heidelberg; 2013:2460-2466. http://dx.doi.org/10.1007/978-3-642-16712-6_59. 10.1007/978-3-642-16712-6_59.

57. Burke KS, Parul D, Reddish MJ, Dyer RB. A simple three- dimensional- focusing, continuous- flow mixer for the study of fast protein dynamics. *Lab on a Chip; Lab Chip*. 2013;13(15):2912-2921.

58. Shastry MCR, Luck SD, Roder H. A continuous- flow capillary mixing method to monitor reactions on the microsecond time scale. *Biophys J*. 1998;74(5):2714-2721.

59. Hertzog D, Ivorra B, Mohammadi B, Bakajin O, Santiago J. Optimization of a microfluidic mixer for studying protein folding kinetics. *Anal Chem*. 2006;78(13):4299-4306.

60. Kise DP, Magana D, Reddish MJ, Dyer RB. Submillisecond mixing in a continuous-flow, microfluidic mixer utilizing mid-infrared hyperspectral imaging detection. *Lab on a Chip; Lab Chip*. 2013;14(3):584-591.

61. Lakowicz JR. *Principles of fluorescence spectroscopy*. 3rd ed.. ed. New York: New York : Springer; 2006.

62. Eftink MR. The use of fluorescence methods to monitor unfolding transitions in proteins. *Biophys J*. 1994;66(2):482-501.

63. Desamero R, Rozovsky S, Zhadin N, McDermott A, Callender R. Active site loop motion in triosephosphate isomerase: T-jump relaxation spectroscopy of thermal activation. *Biochemistry (N Y)*. 2003;42(10):2941-2951.

64. Petersen NO. Topics in fluorescence spectroscopy, vol 3, biochemical applications. *J Am Chem Soc*. 1994;116(11):5024.

65. Wiederschain G. The molecular probes handbook. A guide to fluorescent probes and labeling technologies. *Biochemistry Moscow*. 2011;76(11):1276-1276.

66. Weiss S. Measuring conformational dynamics of biomolecules by single molecule fluorescence spectroscopy. *Nat Struct Biol*. 2000;7(9):724.

67. Diez M, Zimmermann B, Michael Börsch, et al. Proton- powered subunit rotation in single membrane-bound F0F1-ATP synthase. *Nature Structural & Molecular Biology*. 2004;11(2):135.

68. Rob T, Wilson DJ. Time- resolved mass spectrometry for monitoring millisecond time- scale solution- phase processes. *European journal of mass spectrometry (Chichester, England)*. 2012;18(2):205.

69. Kay LE. NMR studies of protein structure and dynamics. *Journal of Magnetic Resonance*. 2011;213(2):477-491.

70. Ohki S, Kainosho M. Stable isotope labeling methods for protein NMR spectroscopy. *Prog Nucl Magn Reson Spectrosc*. 2008;53(4):208-226.

71. Meierhofer D, Wang X, Huang L, Kaiser P. Quantitative analysis of global ubiquitination in HeLa cells by mass spectrometry. *Journal of proteome research*. 2008;7(10):4566.

72. Komander D, Clague MJ, Urbé S. Breaking the chains: Structure and function of the deubiquitinases. *Nature reviews.Molecular cell biology*. 2009;10(8):550.

73. Thrower JS, Hoffman L, Rechsteiner M, Pickart CM. Recognition of the polyubiquitin proteolytic signal. *EMBO J*. 2000;19(1):94-102.

74. Hofmann RM, Pickart CM. Noncanonical MMS2- encoded ubiquitin- conjugating enzyme functions in assembly of novel polyubiquitin chains for DNA repair. *Cell*. 1999;96(5):645-653.

75. Galan J-, Haguenauer-Tsapis R. Ubiquitin Lys63 is involved in ubiquitination of a yeast plasma membrane protein. *EMBO J*. 1997;16(19):5847-5854.

76. Stegmeier F, Rape M, Draviam VM, et al. Anaphase initiation is regulated by antagonistic ubiquitination and deubiquitination activities. *Nature*. 2007;446(7138):876.

77. Haglund K, Dikic I. Ubiquitylation and cell signaling. *EMBO J*. 2005;24(19):3353-3359.

78. Edelmann MJ, Kessler BM. Ubiquitin and ubiquitin- like specific proteases targeted by infectious pathogens: Emerging patterns and molecular principles. *BBA - Molecular Basis of Disease*. 2008;1782(12):809-816.

79. Cstorer A, Ménard R. 33] catalytic mechanism in papain family of cysteine peptidases. *Meth Enzymol*. 1994;244:486-500.

80. Edelmann MJ, Iphöfer A, Akutsu M, et al. Structural basis and specificity of human otubain 1-mediated deubiquitination. *Biochem J*. 2009;418(2):379.

81. James TW, Frias-Staheli N, Bacik JP, et al. Structural basis for the removal of ubiquitin and interferon-stimulated gene 15 by a viral ovarian tumor domain-containing protease. *Proc Natl Acad Sci U S A*. 2011;108(6):2222-2227.

82. Frias-Staheli N, Giannakopoulos NV, Kikkert M, et al. Ovarian tumor domain- containing viral proteases evade ubiquitin- and ISG15-dependent innate immune responses. *Cell Host & Microbe*. 2007;2(6):404-416.

83. van Kasteren P,B., Bailey-Elkin B, James TW, et al. Deubiquitinase function of arterivirus papain- like protease 2 suppresses the innate immune response in infected host cells. *Proc Natl Acad Sci U S A*. 2013;110(9):E838.

84. Rumpf S, Jentsch S. Functional division of substrate processing cofactors of the ubiquitin-selective Cdc48 chaperone. *Mol Cell*. 2006;21(2):261-269.

85. Messick TE, Russell NS, Iwata AJ, et al. Structural basis for ubiquitin recognition by the Otu1 ovarian tumor domain protein. *J Biol Chem*. 2008;283(16):11038-11049.

86. Mark BL, Khajehpour M. Unpublished observations. .

87. Neubauer P, Hofmann K, Holst O, Mattiasson B, Kruschke P. Maximizing the expression of a recombinant gene in escherichia coli by manipulation of induction time using lactose as inducer. *Appl Microbiol Biotechnol*. 1992;36(6):739-744.

88. Gasteiger E, Hoogland C, Gattiker A, et al. *Protein identification and analysis tools on the ExPASy server*. Springer; 2005.

89. Swiss Institute of Bioinformatics. ExPASy protparam tool. http://web.expasy.org/protparam/. Accessed June, 2015.

90. Rabhi I, Guedel N, Chouk I, et al. A novel simple and rapid PCR- based site-directed mutagenesis method. *Mol Biotechnol*. 2004;26(1):27-34.

91. Hospenthal M, Mevissen TE, Komander D. Deubiquitinase- based analysis of ubiquitin chain architecture using ubiquitin chain restriction (UbiCRest). *Nature Protocols*. 2015;10(2):349-361.

92. Riddles PW, Blakeley RL, Zerner B. Ellman's reagent: 5,5′-dithiobis(2-nitrobenzoic acid)—a reexamination. *Anal Biochem*. 1979;94(1):75-81.

93. Ellman GL. Tissue sulfhydryl groups. *Arch Biochem Biophys*. 1959;82(1):70-77.

94. Riener C, Kada G, Gruber H. Quick measurement of protein sulfhydryls with ellman's reagent and with 4,4′-dithiodipyridine. *Anal Bioanal Chem*. 2002;373(4):266-276.

95. Egwim IOC, Gruber HJ. Spectrophotometric measurement of mercaptans with 4,4′-dithiodipyridine. *Anal Biochem*. 2001;288(2):188-194.

96. Grassetti DR, Murray JF. Determination of sulfhydryl groups with 2,2'- or 4,4'-dithiodipyridine. *Arch Biochem Biophys*. 1967;119(1):41.

97. Riddles PW, Blakeley RL, Zerner B. Reassessment of ellman's reagent. *Meth Enzymol*. 1983;91:49.

98. Regino CAS, Richardson DE. Bicarbonate- catalyzed hydrogen peroxide oxidation of cysteine and related thiols. *Inorg Chim Acta*. 2007;360(14):3971-3977.

99. International Union of Pure, Applied Chemistry. Commission on Equilibrium Data, Serjeant EP, Dempsey B, International Union of Pure, Applied Chemistry. Commission on Electrochemical Data. *Ionisation constants of organic acids in aqueous solution.* Pergamon Press; 1979. https://books.google.ca/books?id=__8oAQAAMAAJ.

100. Ajish Kumar K , Haj-yahya M, Olschewski D, Lashuel H, Brik A. Highly efficient and chemoselective peptide ubiquitylation. *Angewandte Chemie International Edition*. 2009;48(43):8090-8094.

101. HU M, LI P, LI M, et al. Crystal structure of a ubp- family deubiquitinating enzymen in isolation and in complex with ubiquitin aldehyde. *Cell*. 2002;111.

102. Geurink PP, Van Tol BDM, Van Dalen D, et al. Development of diubiquitin- based FRET probes to quantify ubiquitin linkage specificity of deubiquitinating enzymes. *ChemBioChem*. 2016;17(9):816-820.

103. AppliChem. *Biological buffers.* AppliChem; 2008. https://www.applichem.com/fileadmin/Broschueren/BioBuffer.pdf.

104. Mohan C. *Calbiochem buffers booklet.* EMD Biosciences, Inc.; 2003. http://wolfson.huji.ac.il/purification/PDF/Buffers/Calbiochem_Buffers_Booklet.pdf.